FACULTY OF SCIENCE AND TECHNOLOGY

MASTER THESIS

Study programme / specialisation:
Reservoir Engineering

The spring semester, 2022

Open / Confidential

Author: Tongtong Yu

Tongtong Yu

.....

(signature author)

Course coordinator: Øystein Arild

Supervisor(s): Raoof Gholami

Thesis title:
Fluid-Rock Interactions for CO_2 Geological Storage in Chalk

Credits (ECTS): 30

Keywords:
CO_2
Storage
Chalk
Calcite
Precipitation
Porosity
Permeability

Pages: 66

Stavanger, Norway
15th June 2022

Abstract

CCS has been recognized as an effective strategy to limit the temperature rise to 1.5 °C by 2050 under the Paris Agreement. As a result, more than 50 CCS pilot or large-scale projects have been commissioned in recent decades, mainly targeting sandstone reservoirs given their favorable petrophysical properties. Although many discussions and practical procedures have been developed, large-scale CO_2 storage in carbonates has not yet been implemented. This study attempts to evaluate the feasibility of CO_2 storage in chalk formations. The main objective is to evaluate the changes in the storage capacity (porosity) and injectivity (permeability) over time during and after CO_2 injection. For this purpose, a series of laboratory tests were carried out on Stevns Klint chalk from Denmark, after exposure to dry/wet CO_2 for a period of 37 days under a pressure of 15 MPa and a temperature of 50 °C. The results obtained indicated significant removal of Ca^{2+} ions from the solution and large precipitation of calcite in the pore structure, which reduced porosity and permeability over time. It was found that chalk may not the best storage site given the rapid reduction in porosity and permeability which can cause complication in well injectivity over time.

Key Words: CO_2, Storage, Chalk, Calcite, Precipitation, Porosity, Permeability

Acronyms & Abbreviations

ACC	Amorphous Calcium Carbonate
BET	Brunauer, Emmett and Teller (Theory)
$CaCO_3$	Calcium Carbonate
CaO	Calcium Oxide
CCS	Carbon Capture and Storage
CH_4	Methane
CO_2	Carbon Dioxide
DDC	Dissolution Diffusion Convection
DSC	Differential Scanning Calorimetry
ECBM	Enhanced Coalbed Methane (Production)
EDS	Energy Dispersion Spectrum
EOR	Enhanced Oil Recovery
GHG	Green House Gases
ICDD	International Centre for Diffraction Data
LPG	Liquefied Petroleum Gases
NMR	Nuclear Magnetic Resonance
NO_2	Nitrous Oxide
PM	Particulate Matter
RF	Radiofrequency
$scCO_2$	Supercritical CO_2
SEM	Scanning Electron Microscopy
TGA	Thermogravimetric Analysis
UCS	Uniaxial Compressive Strength
XRD	X-ray diffraction

Table of Content

Table of Figures

List of Tables

1. Introduction

1.1. Background

The year 2021 just passed was the sixth hottest year since 1880 (NOAA National Centers for Environmental Information, 2022). Our climate change caused by human activities is largely due to the emissions of greenhouse gases (GHGs), among which carbon dioxide as by-product from combustion of fossil fuels is the decisive factor (The Climate Reality Project, 2021). At the same time, global energy demand will increase 50% with the growth of population and economy (U.S. Energy Information Administration, 2021), which will lead to continuous rising in CO_2 emissions.

As a result, many approaches have emerged and Carbon Capture and Storage (CCS) technology, as a practical method, has become a key option to mitigate the effect of climate change through reducing anthropogenic CO_2 emissions to the atmosphere, and even the only way to decarbonize some of the world's critical industrial sectors including cement, metal production, and waste incineration (SINTEF, n.d.). CCS technology is the process of capturing CO_2 produced by industrial processes, transporting to underground sequestration site to store CO_2 permanently and safely. The process is shown in Figure 1 below (Norwegian Petroleum, 2020). It includes three major steps: capture, transportation and storage.

Storage, as the last step of CCS project, is the crucial factor of deciding whether a CCS project if successful or not. It mainly depends on the storage stage considering how well the injected CO_2 can be stored in the geological formations by two crucial points: safe and effective. It can be evaluated from aspects of the capable injection amount of CO_2 and time period the site could hold the stored CO_2 (Hepple & Benson, 2005). The storage step will be the focus in this paper and the issues may happen will be discussed.

The storage sites having enough capacities are mainly chosen from depleted oil & gas reservoirs, saline aquifers, unmineable coal seams and deep oceans. Within the known storage options, storage in deep oceans has not been tested and for unmineable coal seams, pilot-scale testing has not been successful so far. While storage in both depleted oil & reservoirs and saline aquafers are demonstrated successful methods. For depleted oil and gas reservoir, the strategy is storing CO_2 in the pore space of reservoir rocks for hundreds or thousands of years and it is similar in saline aquifers. The difference between them is the original fluid in depleted oil and gas reservoir could be oil, gas, water or the mixture of these three while in saline aquifers, it was brine. CO_2 is usually injected at the depth of deeper than 800 m for the pressure and temperature at that depth will make CO_2 at the state of supercritical CO_2, a state having higher density and lower viscosity. The choose of this supercritical state is related to two basic properties: porosity and permeability. The ratio of pore volume to total rock volume is known as porosity. It represents for how

much CO_2 can be stored in the reservoir and is the decisive factor of storage capacity in CCS project. For CO_2 with higher density, same amount of CO_2 will occupy smaller volume so that bigger amount of CO_2 can be stored in the reservoir. As to permeability, an indication of the ability for fluids flowing through the rock, is closely related to porosity, the shape of the pores, how the pores connect to each other, pressure inside the rock, fluid physical properties, etc. (Wikipedia, 2022b). For CO_2 with lower viscosity, it has stronger ability of going through reservoir rocks (Bandilla, 2020).

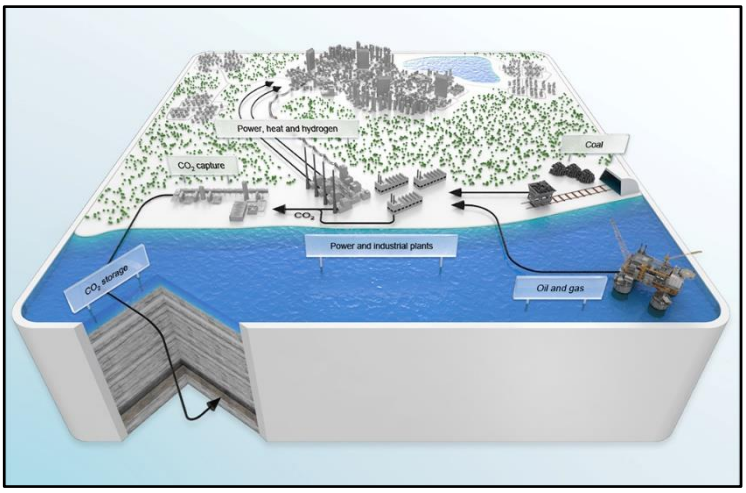

Figure 1. Carbon Capture, Transport and Storage Process (source: norskpetroleum.no).

After CO_2 is injected into the geological formations, it will go upwards because density of $scCO_2$ is lower than water and its buoyancy action. While at the same time, the fluid-rock system will go through different storage mechanisms including structural storage, residual storage, dissolution storage and mineral storage. CO_2 is getting less mobile and the risk of CO_2 leakage is lower during these processes (di Gianfrancesco, 2017). The system is therefore more stable and in the trend towards equilibrium.

1.2. Motivation of this Study

During these storage mechanisms, injected CO_2 may interfere the initial equilibrium of the underground environment and cause chemical interactions with formation fluids and rock minerals, including siliciclastic or carbonate sedimentary rocks, once it comes into contact with rocks. These interactions will change the reservoir environment not only towards the positive direction to mineral storage mechanism, but also have negative effects towards CO_2 trapping in geological sites. During which dissolution of CO_2, acidification of water, declination of pH value, solubility of rock minerals into the brine and subsequent precipitation of new carbonate minerals may be triggered to a new equilibrium trend. Both of temperature and pressure have

influence on solubility of CO_2 in brine so to change the acidity of carbonic acid and then affect the degree of corrosion (Lin et al., 2022). Rock system in the reservoir is changing at the same time because of the dissolution and precipitation of rock minerals and may lead to impact on porosity and permeability both in cap rock and host rock, as well as pore structure including mineralogy, roughness of pore surfaces, pore throat size and also the dynamic properties including wettability, relative permeability capillary pressure and so on. All these parameters will gradually have varying degrees of influence on from capillary pressure trapping efficiency, CO_2 plume size, to storage capacity (H. Wang et al., 2021). Thus, may negatively affect seal integrity and may cause leakage, as well as cause fault reactivation or even storage layer collapse during expected CO_2 storage time in more severe cases (Y. Zhang et al., 2020). Leakage into atmosphere will weaken the effectiveness of CCS process, waste money and time costs of CCS project and aggravate greenhouse effect. While leakage into potable aquifers will cause contamination, acting direct or indirect impacts on water that might be used by humans. Safety and security of the whole CCS process is crucial to both human beings and environment. These need to be controlled as well as guaranteed to minimize the uncertainties may happen during its storage period.

On the other hand, the present depleted reservoirs still have significant amount of oil or gas left due to various reasons. And they may be recoverable in the future with the development of recovery technology or the increase of oil price. It is also essential to study into how CO_2 can have impact in reservoir settings in this respect (Advanced Resources International, 2000).

Therefore, the confirmation of feasibility of storage sites should be done before implementation of CCS technology. In order to get a more accurate feasibility evaluation of the CO_2 trapping condition and to ensure a safe, stable and successful CCS project, risks should be analyzed beforehand so that they could be eliminated or minimized in the actual project in progress. The risks are involved in different stages during CCS project and related to both of geological and operational uncertainties (Amini et al., 2012). The interactions between $scCO_2$ and formation rocks is one of the most important aspects among the whole process and the understanding of it should be studied and clarified to help predict how the formation rock will be and the reservoir changing trends after CO_2 is stored in hundreds even thousands of coming years. There are four important techniques that can be used for this research: 1. laboratory experiments, 2. natural analogues, 3. demonstration, fields experiment and monitoring and 4. geochemical and coupled modeling (Gaus, 2010). Among which laboratory experiments is one of them to assess CO_2-rock interactions by providing experimental data and direct observation at a very detailed level.

1.3. Study Results from Recent Articles

Many studies into how CO_2 effects the properties of rocks under different scenarios have been carried out. For example, in tight sandstone, after CO_2-water-rock minerals reactions, porosity and permeability increased due to mineral dissolution of

calcite, dolomite and feldspar inside the pore throat (Lin et al., 2022). Sun et al. got the similar trend of porosity variation in tight sandstone with 34.9% feldspar and dolomite and it's more obvious in large-size pores compared to small pores. Furthermore, they looked into relative permeabilities: relative CO_2 permeability is lower after corrosion but for water permeability, it could increase or decrease, depending on CO_2 saturation in two-regime flow (Y. Sun et al., 2021). Zhao et al. and Li et al. studied the relationship between pore structure and permeability but got opposite permeability results. From Zhao et al.'s article, the reduction of distribution probability of large throats (0.44-1μm) was the main reason for permeability decrease after CO_2-water-rock (with 39.3 % quartz & 36.1 % feldspar) interaction. And it's severe with higher pressure and temperature (Zhao et al., 2015). But permeability in tight sandstone gave an increased result according to Li et al.'s experiments. That was because large pores (10-50 μm) were generated due to dissolution of carbonate & feldspar after CO_2-brine-rock interactions. Increased soaking pressure and CO_2 concentration may significantly increase porosity and permeability (Li et al., 2020). Wettability is another crucial parameter should be looked into for CO_2 storage. Iglauer found that CO_2-wettability increased with pressure, brine salinity and particularly hydrophobicity of the rock surface (Iglauer, 2017). The same impact of pressure is also shown in oil-wet surface of sandstone sample in Ameri et al.'s study. But for water-wet sample, pressure had little impact on wettability change and the contact angle decreases for increasing brine salinity (Ameri et al., 2013). In research from Foroutan et al., injection rate was considered a controllable and decisive factor affecting physical-mechanical characteristics of formation rocks. Three different kinds of specimens were injected by CO_2-enriched brine using two injection rates. For pure calcite, permeability enhancement was more obvious under higher injection rate but it's the opposite for calcite-cemented and quartz-cemented sandstone. And fracture channelization was significant in limestone under both injection rates (Foroutan et al., 2021). Likewise, F. Wang et al. studied into impact induced by CO_2 injection rate and combined laboratory experiments together with simulation. They got the result that the higher the CO_2 injection rate is, the larger the enhancement effect of mechanical response which has a positive influence on CO_2 injection, migration and storage in the reservoir (F. Wang et al., 2021). Impurities in CO_2 stream could be another factor effecting physical properties. But it had a negative effect on sandstone: both of grain diameter and permeability decreased (permeability decreased by 41.6%) after CO_2 injection (Aminu et al., 2018). Not only for sandstone reservoirs, carbonate reservoirs are now catching higher attention as potential CCS sites and being studied from multiple aspects (Crockford & Telmer, 2011; Tartarello et al., 2017; H. Wang et al., 2021; Y. Zhang et al., 2020).

From the researches above, the effects of CO_2-brine-rock interactions from different researches can be different, even opposite according to factors including massive diversity of different reservoirs (mineralogy and physicochemistry), CO_2 concentration, CO_2 injection rate, interaction pressure & temperature and also different research methods. So far, there is no definitive conclusion and explanation

from researchers as to whether CO_2-fluid-rock interactions will affect storage capacity of a reservoir positively or negatively, and how will the physical rock properties like porosity and permeability and dynamic properties like wettability, relative permeability and capillary pressure change after CO_2 is injected. And it's the same situation to the theory on how these properties will influence CO_2 storage capacity and long-term safety in subsurface storage sites. The situation in the saline aquafers and depleted oil & gas reservoirs is not clear up to now and the data base is not yet sufficient. Therefore, in order to elucidate the alteration trend of carbonate rocks induced by injected $scCO_2$ and add further data to the existing data base, more investigations into CO_2-fluid-carbonate rock interactions are needed. A laboratory experiment is presented in this study observing alterations of chalk after exposure to $scCO_2$. Comparisons including porosity, pore size distribution, permeability, specific surface area, thermostability, mineralogy, uniaxial compressive strength (UCS) of the chalk samples, and pH value and ion composition of interaction solution are conducted to identify the alteration. Whilst carbonate reservoirs are found storing significant proportion of world's oil reserve and the chalk reservoirs in the North Sea pioneered the petroleum in Norway (Faleide et al., 2015), the study into carbonate reservoirs is significant to Norwegian oil industry.

1.4. Thesis Structure

This paper is divided into 5 chapters. **Chapter 1** is the introduction of this study's background and explanation of why more evaluations of CO_2-brine-rock interactions are needed: elucidation of necessity and existence of various conclusions from part of the latest research surveys. **Chapter 2** is the literature review, including the overview of the environment and energy situation, introduction to the CCS project and the interactions may happen in the reservoir after CO_2 injection. **Chapter 3** is the methodology: introduction of the rock used in this study, procedure of the experiment, methods of property measurements and steps of each individual tests. And the results and discussion of each individual test are stated in **Chapter 4** on alteration about rock and solution properties. The last part **chapter 5** is the conclusions of this study and further works needed.

2. Review of Literature

2.1. Introduction

Because of the continuous rising of energy consumption all over the world, which leads to GHG emissions and result in global warming, CCS technology is playing an important role of reducing carbon emissions through 3 main steps: capture, transportation and storage. In this chapter, global energy and environment situation will be firstly introduced, followed by the CCS process of each stage, and the interactions may happen after CO_2 is injected into the formations underground will be discussed at the end.

2.2. Global Energy & Environment Situation

In 2020, global energy consumption was 557.1 EJ. Asia Pacific was responsible for 45% of total consumption, followed by North America and Europe of 19% and 13.8%. The top three shares of energy resources were held by oil, coal and natural gas, accounting for 31.2%, 27.2% and 24.7% respectively (BP p.l.c., 2021). Though energy consumption per capita in 2020 was 71.5 GJ/head, energy poverty still exists, especially in Asia and sub-Saharan Africa. Driven by population growth (the world's population is estimated to be 9.8 billion in 2050 (World Mapper, n.d.), 1.9 billion more than it is now), improvement in standard of living in non-OECD countries and also economy and industry development, energy need continues to increase worldwide. Predicted by the US Energy Information Administration (EIA), global energy demand will increase nearly 50% by year 2050 compared to 2020, mostly in Asian developing countries.

Although increasing electricity will mainly be generated by renewable energy of 27% of energy use, and share of coal consumption declines after 2030, oil and natural gas production will still continue growing in Asian countries to meet the demand of energy consumption (U.S. Energy Information Administration, 2021). Data in the same trend is also provided by International Energy Agency (IEA) illustrated in Figure 2. In the Stated Policies Scenario, prediction of change in consumption of fossil fuels including coal, oil and gas from year 2019 to 2040 shows that coal is relatively speaking much less important than previous but oil and gas are still playing an important role worldwide in the near future. Fossil fuels apply for 83.1% of energy consumption in 2020 (BP p.l.c., 2021), which is the same as it was 25 years ago and it is predicted that they will still dominate world's energy use in 2050 accounting for the percentage of 74% (Nyquist, 2016), without obvious drop in ratio. Within all types of energies, renewables increased by the largest ratio of 9.7% --is estimated being the most used energy source of 28% in 2050 (Kahan, 2019)-- followed by hydroelectricity of 1% and fossil fuels including oil, coal and natural gas at the decreasing ratio of 9%, 4.2% and 2.3% respectively (BP p.l.c., 2021). The fact is that

the share of fossil fuels accounts for the largest proportion can't be easily reduced in decades.

More renewable energy like wind power, solar energy, geothermal energy, etc. will be used and the efficiency will be improved due to more advanced technology in the future but at the same time the world's population is estimated 24% growth in 2050. That means global need for energy will keep rising for a long time in the future. As a result, carbon emission will increase with the global energy need, keeping at the same trend. 87% of the emissions of man-made carbon dioxide are from combustion processes of fossil fuels in power plants and homes for electricity and heat. Other anthropogenic CO_2 sources are changes to land usage like the clearing of forests or draining of wetlands which accounts for 9% and the rest 4% is from other industrial processes like cement production (ECMWF, 2017). From "Statistical Review of World Energy 2021" by BP, global carbon dioxide emission was 32 billion tonnes in 2020, firstly showing an obvious declination of 6.2% since 1945. The largest share of the decline in CO_2 emission was contributed by Europe of 12.3%. North America contributed the second largest declination of 12.1%. Until 2050, the forecast of CO_2 emission will increase to 43.08 billion tonnes (Tiseo, 2020).

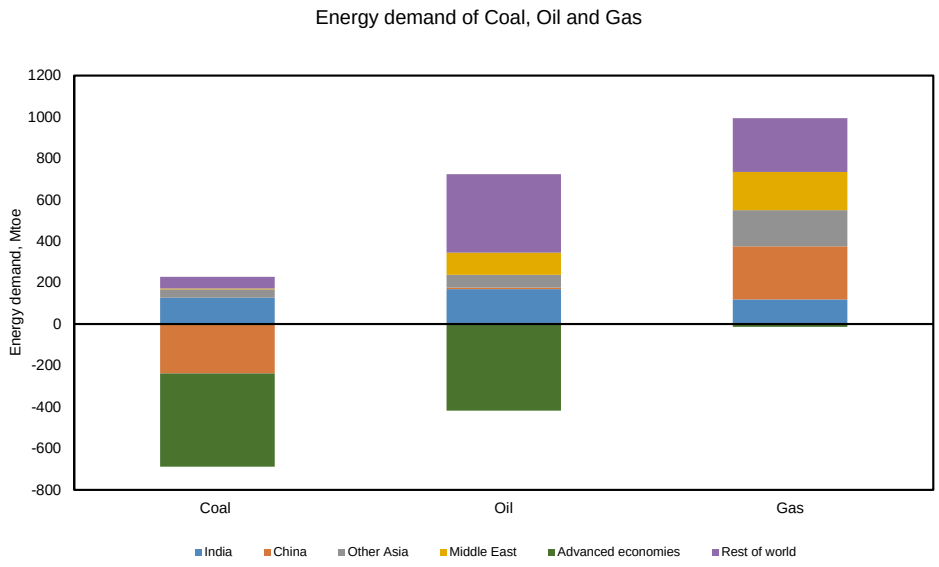

Figure 2. Change in Total Primary Energy Demand in Selected Regions in the Stated Policies Scenario, 2019 - 2040 (data source: iea.org).

Our climate change caused by human activities is largely due to the emissions of greenhouse gases (GHGs) including carbon dioxide (CO_2), methane (CH_4), nitrous oxide (NO_2) and fluorinated gases (EPA, n.d.). And the environmental effect of global warming is resulted mostly from carbon emissions as by-product from combustion of fossil fuels for electricity, industry and transportation (The Climate Reality Project, 2021), which was proven by scientists over the past century. It can lead to the increasing likelihood of sea level rising, droughts and other severe weather patterns.

But effects of carbon emissions will not stop at the environment, it will cause a higher risk of us human beings getting cancer and respiratory diseases due to increased smog and air pollution (Young Upstarts, 2021). In order to reduce the effects of climate change effectively and reach a mandatory implementation by individual countries, Paris Agreement was negotiated by 196 parties and adopted in 2015. The goal is to limit the increasing temperature within 1.5 °C (2.7 °F) by middle of the 21st century compared to pre-industrial period. Now the Paris Agreement has been successfully used as a standard for forcing the parties ratified the agreement to reduce the emission of CO_2 and onto other climate actions (Wikipedia, 2022a). Though it gave a surprising result of carbon emission in 2020, it happened in the background of global pandemic which led to economic drop. Therefore, more efforts need to be done in the following years.

2.3. Carbon Capture and Storage (CCS)

Towards reduction of CO_2 emissions, there are many measurements can be done. From personal contributions like reducing energy use at home, alternatives to driving, support clean energy sources, to establishment of more strict policies like imposing carbon tax or fees towards factories, transportation industry and other related areas. Moreover, carbon capture and storage (CCS) is recognized as the most effective way for lowering CO_2 emissions caused by humans in today's situation (Carbon Capture & Storage - CCS Research from SINTEF, n.d.). CCS is a technology of storing the carbon dioxide which is captured and separated from electricity generation and industrial productions in geological site underground. There are three main steps involved in this process: capture, transportation and storage.

2.3.1. Capture

Capture is the first step of CCS operation which prevents CO_2 being emitted to the atmosphere. It happens at the significant emitters -- stationary sources of coal or gas power plants and industrial processes like cement, ammonia, pulp and paper, chemicals, and steel production. Among which fossil fuel-fired power plants generate a larger percentage of CO_2 emissions than any other industry so it has the potential of great reduction of CO_2 emissions compared to other sections. To many of the industrial processes, CCS is the only approach for reducing CO_2 emission efficiently. During capture process, impurities in the emissions including moisture, acid gases, solid-phase particulate matter (PM) and metal aerosols need to be removed, in order to minimize the negative effects induced by impurities during the following compression, transport and storage process (Finney et al., 2019). Separation of carbon dioxide is therefore operated at this step. Methods of capturing technologies can be mainly categorized into three basic types: separating CO_2 from fuel before combustion (pre-combustion separation), separating from the exhaust gases after combustion (post-combustion separation) and combustion with pure oxygen (oxy-fuel combustion) according to when CO_2 is removed from emission gases.

In **pre-combustion** separation, the fuel is converted into a gaseous mixture of hydrogen and CO_2. Then hydrogen can be burnt as fuel without producing any CO_2 and CO_2 part is processed to next stage of transportation. Pre-combustion separation technology is used in industrial productions while the fuel conversion step in pre-combustion separation is more complex in post-combustion separation, this technology is more difficult applied in existing power plants. During **post-combustion** separation process, CO_2 is separated from gas mixture after fuel combustion. CO_2 can be captured using a liquid solvent or other methods. After being absorbed by the solvent, a higher purity of CO_2 could be obtained by heating the solvent. The CO_2 obtained by this method could be used in beverage and food production. Post-combustion separation technology is the most mature one among these three methods (Zero Emission Resource Organisation, 2016). For **oxy-fuel combustion**, oxygen is used as fuel in combustion process rather than air. So that high purity of CO_2 could be obtained after combustion from exhaust gas which is the mixture of mainly water vapor and CO_2 (Global CCS Institute, n.d.-a).

2.3.2. Transportation

After capturing, it comes to the second step of CCS process – transportation. CO_2 needs to be transported to geological storage site for indefinite-time period objective (except capture facilities located very close to the eventual storage site). CO_2 can be transported in gas, liquid or solid state by methods of rail and road tankers for small-scale transportation, or by pipelines and shipping for large-scale transportation. Pipelines and shipping are methods for transporting gaseous and liquid CO_2 in commercial scale. CO_2 need to be compressed before transported because large volume of CO_2 will need large scale of facilities. Though solid is the smallest volume for CO_2, more energy as well as cost are needed in the process of solidification (Doctor et al., 2018). Therefore, when CO_2 needs to be transported long distance overseas, it can be transported in the form of compressed gas at the pressure above 8 MPa by pipelines, or in liquid form at the pressure of 0.7 MPa by ship in the same way with liquefied petroleum gases (LPG) (Green Facts, 2005). Besides, CO_2 is usually transported in supercritical state, in which it has the density of a liquid and the viscosity of a gas. At this state, CO_2 has higher density of 500-700 kg/m^3 which could reduce the required transport volume and lower viscosity which could reduce transmission energy losses (Bandilla, 2020). Also, CO_2 needs to be dried to decrease the water percentage in order to decrease the corrosion rate of transportation facilities like pipelines. The transportation infrastructure will continue being built and is estimated 100 times larger than current condition in 30-40 years (Global CCS Institute, n.d.-b).

2.3.3. Storage

2.3.3.1. Storage sites

Storage, as the last step of CCS, keeps captured CO_2 in the geological storage sites from emitting into the atmosphere. There are many sedimentary regions suitable for CO_2 storage, which have enough capacities: depleted oil and gas reservoirs, saline aquifers, unmineable coal seams and deep oceans.

Depleted oil and gas reservoirs are one of the prospective geological structures for CO_2 storage. The first advantage of them is that the oil and gas reservoirs were studied in depth and the characteristics and properties of the reservoirs were well understood, which are essential for the implementation of CCS project and the safety of long-time storage. And for the future trends of reservoirs, simulation methods developed can be used to predict the movement, displacement and trapping of hydrocarbons. The second advantage is the reservoirs' integrity is guaranteed because oil and gas has been trapped over millions of years, making it safe for CO_2 storage. The next point is that the infrastructures already constructed can be used in CO_2 injection process. Finally, CCS project can also be optimized to enhance oil and gas in the future (Metz et al., n.d.).

Saline aquifer is a geological formation of porous sedimentary rocks containing salt water and they are usually deeper than fresh water aquifers. These aquifers are widespread all over the world so it will make the transportation process convenient if they're used as storage sites. But the study into saline aquifers is not enough so far and will cause uncertainties after CO_2 injection (Definition > Saline Aquifer, n.d.). The Sleipner Project in the North Sea is the best example for CO_2 storage in a saline aquifer. From a hydrodynamic point of view, saline aquifers and reservoirs are at the same level. Porosity and permeability characteristics are similar but the type of fluids present in the pore space are different. Another important distinction between reservoirs and saline aquifers is the spatially discrete and discontinuous nature of the oil and gas reservoirs, but the opposite of the aquifers (Bachu et al., 2007).

Unmineable coal seams are another promising choice for CO_2 storage because there are large unmineable coal seams can store large volumes of CO_2 (90 billion metric tons) directly from power plants with long-distance transportation. And CO_2 can be used for enhanced coalbed methane production (ECBM). At the same time, at least two or three molecules of CO_2 can be adsorbed onto the coal when one molecule of methane is released. But it was found that CO_2 storage in unmineable coal seams may have the potential of causing environmental issues (Hedges et al., 2007).

Besides geological storage, an alternative of **deep ocean** has possibility of CO_2 storage. This kind of sites are in enclosed basins on the deep (> 4 km) and very deep (> 6 km) ocean floor. If liquid CO_2 is placed in the trench under 6 km depth, it would be 7% denser than seawater and could stay at that depth permanently as a lake of liquid CO_2. And it has the possibility of becoming hydrate solid in the future, which could

separate itself better from seawater. The deep ocean sites have a vast capacity of CO_2 storage all over the world. For example, the Indonesian Sunda trench has the capacity for 19,000 Gt of liquid CO_2 and the Puerto Rico trench has the capacity of 24,000 Gt of liquid CO_2. But it is still considered an infeasible option because of possible ocean acidification, negative impacts on marine species, risk of CO_2 release due to seismic activities (Goldthorpe, 2017) and technological challenges.

For a suitable geological storage site, the following basic conditions need to be met: appropriate capacity, injectivity, and containment. These three points are main storage issues need to be considered. Capacity is the room in storage sites for CO_2 storing, measuring CO_2 storage volume. Injectivity evaluates how well it injects CO_2 into the storage sites at a certain injection rate. Containment needs a sealable structure and a stable geological environment that could guarantee the integrity and safety of the storage site (Metz et al., n.d.), so that CO_2 won't migrate to other geological formations or even leak out during the whole CCS project.

2.3.3.2. Key aspects

1 - Capacity

Intuitively, storage capacity is a volumetric (spatial) term (Bachu et al., 2007). In comparison to saline aquifers and unmineable coal seams, estimating the CO_2 storage capacity in oil and gas reservoirs is the easiest since they have previously been discovered and produced. In these reservoirs, storage capacity mainly depends on both of the volume of pore space and the reservoir permeability (D. Zhang & Song, 2014). And the capacity can be calculated using rock volume, porosity, original oil or gas in place, recovery factor, in-situ CO_2 density, as well as pressure and temperature. The theoretical mass CO_2 storage capacity in a reservoir can be calculated by the equation:

$$M_{CO_2 t} = \rho_{CO_2 r}\left[\frac{R_f OOIP}{B_f} - V_{iw} + V_{pw}\right] \quad \text{Eq. 1}$$

for oil reservoirs, and by the equation

$$M_{CO_2 t} = \rho_{CO_2 r} R_f (1 - F_{IG}) OGIP\left[\frac{(P_s Z_r T_r)}{(P_r Z_s T_s)}\right] \quad \text{Eq. 2}$$

for gas reservoirs. In which R_f is the recovery factor, B_f is the formation volume factor that brings the oil volume from standard conditions to in situ conditions, V_{iw} is the injected water volume and V_{pw} is the produced water volume, r and s donate conditions of reservoir and surface, and P, T, and Z represent for pressure, temperature and gas compressibility factor separately (Bachu et al., 2007). Capacity dominates in the in the site selection phase (Ringrose, n.d.).

2 - Injectivity

Injectivity (ability to inject a fluid) is a time-dependent (flow rate) concept. It is

identified as a pre-requisite for CO_2 geological storage. Injectivity is influenced by permeability, relative permeability, pressure, temperature, porosity, brine salinity, reservoir volume and fluid properties (Tawiah et al., 2020). It is widely considered that rocks with permeability no more than 0.1 mD are defined as barriers for fluids to flow. For low permeability rocks, injectivity can be enhanced by well stimulation like rock fracturing or by increasing the number of injection wells (Bachu et al., 2007). Injection pressure, fluid saturation, and fluid mobility (controlled by reservoir porosity and CO_2 relative permeability under reservoir condition) all have influence on injection rate. Injectivity can be expressed by the equation:

$$I_{inj} = \frac{Q_m}{P_{bh} - P_r} = \frac{m}{t \times \Delta P} \quad \text{Eq. 3}$$

where m is CO_2 mass, t is time, P_{bh} is bottom hole injection pressure, P_r is reservoir pressure. This equation expresses injectivity as the amount of energy necessary to inject a unit mass of CO_2 while removing the complexity induced by PVT effects (Tawiah et al., 2020). Injectivity is the prime condition in the site operation phase (Ringrose, n.d.).

3 - Containment

Once CO_2 is injected into a geological formation as an oil and gas reservoir or saline aquifer, CO_2 can be sequestrated in geological by four mechanisms: structural & stratigraphic trapping, residual CO_2 trapping, solubility trapping and mineral trapping (Ringrose, n.d.). During residual, solubility and mineral trapping, the security and safety of CO_2 geological storage is increasing and the amount of free CO_2 is decreasing. These trapping mechanisms work very slowly, up to hundreds or thousands of years (Bachu et al., 2007).

4 - Trapping mechanisms

Structural and stratigraphic trapping (is also called hydrodynamic trapping (D. Zhang & Song, 2014)) signifies when CO_2 is trapped as gas or in supercritical state under a low-permeability caprock. The sealing capacity of caprock decides the CO_2 sequestration and make it a crucial factor in storage site selection. The principle of it is the physical process of capillary trapping caused by the interfacial tension at the interface between two fluids in a pore space (Ringrose, n.d.). Because CO_2 has a lower density than formation fluid, it will go up because of buoyancy until it contacts caprock and requires a larger capillary entry pressure than the buoyancy or hydrodynamic force. Sedimentary basins' trapping effectiveness is determined by their structure, which can limit fluid flow by dispersing high and low permeability strata across the basin. Because additional trapping mechanisms are coming into play during this time, this mechanism is critical (D. Zhang & Song, 2014).

The second important capillary trapping mechanism is **residual trapping**. When a CO_2 plume migrates upwards, a trail of unconnected CO_2 is trapped in the pore space behind it due to the density difference between CO_2 and formation water, as well as wettability towards these two fluids. This phase is controlled mostly by the wettability, the pore throat size and the interfacial tension. CO_2 is considered as a

non-wetting phase in sandstone reservoirs and partial wetting for carbonate reservoirs (Ringrose, n.d.). According to certain research, not only pore-scale processes, but also injection rate, heterogeneity, and the viscous-gravity force ratio have a substantial influence on the ultimate trapped gas saturation. It can be calculated by dynamic flow simulations or analytical approaches. The residual trapping process is crucial to the migration and distribution of injected CO_2, which could further have impact on the other trapping mechanisms (D. Zhang & Song, 2014).

Solubility trapping is the dissolution process of CO_2 into formation fluids. When CO_2 contacts with formation fluids, it will be dissolved until the system reaches an equilibrium. The solubility of CO_2 in formation water is affected by the reservoir's pressure and temperature, as well as the aqueous phase's salinity (Ahmadi & Chapoy, 2018). Through molecular diffusion, CO_2 dissolves in formation water. At the interface between CO_2 and formation water, the fluid is saturated with water and the concentration of CO_2 in formation water goes down as the distance from CO_2 phase is further. But the high-CO_2-concentration formation water will go down due to its slightly higher density after dissolved with CO_2. After that, low-CO_2-concentration formation water goes up and could be saturated with CO_2 again. This process is called dissolution-diffusion-convection (DDC) process. DDC process could increase the CO_2 solubility into formation water, as well as the storage capacity, thereby reducing the risk of CO_2 migration and leakage (D. Zhang & Song, 2014). This process is complex, and can take thousands of years to complete the whole dissolution process (Lindeberg & Wessel-Berg, 1997), depending on geology and heterogeneity of the reservoir and the defined dissolution rate (Gaus, 2010).

After CO_2 is dissolved in the formation water, it can directly or indirectly interact with metal cations (predominately Ca, Fe and Mg (Rackley, 2017)) in the form of dissolved CO_2 in brine or acidification of the brine (Gaus, 2010) and some fractions of CO_2 can be converted to stable carbonate mineral in the storage sites at the end (Metz et al., n.d.). This process is called **Mineral trapping**, initiated by a serious of geochemical reactions. Some of these reactions are beneficial for CO_2 storage. For example, basaltic rocks show an optimistic storage capacity of CO_2 because of its rapid mineralization of injected CO_2 (Snæbjörnsdóttir et al., 2014) and alumino-silicate minerals are considered as cation donors of carbonates for permanent trapping of CO_2 (Gaus, 2010). And mineral trapping also broadens the scope of CCS by allowing storage in regions where it was previously thought unfeasible (Snæbjörnsdóttir et al., 2020). But part of them can also be disadvantageous to mineral trapping and cause migration of CO_2. The reaction rate in aqueous phase depends on pressure, temperature, pH value and other ions concentration in the fluid. Mineral trapping mechanism is of considerable importance for CO_2 storage but it’s a very slow process due to the low reaction rate and it may take over thousands to millions of years (D. Zhang & Song, 2014).

The four mechanisms should work together to reach the containment goal of increasing storage security and avoiding leakage of CO_2 back to the atmosphere or

into drinking water aquifers. Containment is the basic problem during the site closure and post-closure phase (Ringrose, n.d.).

2.4. Fluid-Rock Interactions

The complex process of CCS project is induced by the complex phase behavior and the interactions between different phases: oil, formation fluid and injected CO_2. CO_2 will be dissolved in formation water and form acidic solution after injected into the reservoir, which happened in solubility trapping process and can be described using the following formulars:

$$CO_2(g) \Leftrightarrow CO_2(aq) \qquad \text{Henry's law} \qquad \text{Eq. 4}$$

$$CO_2(aq) + H_2O(l) \Leftrightarrow H^+ + HCO_3^-(aq) \qquad K_{eq} = 10^{-6.35} \qquad \text{Eq. 5}$$

$$HCO_3^-(aq) \Leftrightarrow H^+ + CO_3^{2-}(aq) \qquad K_{eq} = 10^{-10.33} \qquad \text{Eq. 6}$$

After injecting CO_2 into water, it will be dissolved and result in production of bicarbonate ions, increase of H^+ concentration and decrease of pH value at last. The pH value will decrease to around 3 in reservoirs. In this stage, the situations are different in different reservoirs. When CO_2 is injected into a pure quartz sandstone and saturate the formation water, the following injected CO_2 will build up a separate phase. But when CO_2 is injected into carbonate reservoirs or carbonate cemented sandstone, a separate phase will be formed the time water is saturated with CO_2, which is after carbonated mineral dissolution (Baines & Worden, 2004).

After acidic solution is formed, some kinds of minerals can be dissolved when they are exposed to the solution. Through the interactions between the weak acid H_2CO_3, minerals and free ions in the solution, the system tends to reach an equilibrium. For example, interactions with carbonate minerals will quickly buffer the pH value in solution and render the formation water less acid. The representative chemical reactions may happen in the reservoirs and their typical reaction rates are summarized in Table 1 (Espinoza et al., 2011).

The reaction rate of minerals depends on pressure and temperature, which impact CO_2 solubility in water and result in pH value variation. Solubility of the minerals depends on temperature, pressure, salinity, ions concentration and pH value. Comparing the three formulars may happen within carbonates and their equilibrium constant, $CaCO_3$ is easier to be dissolved when the pH value is lower and $CaCO_3$ could also be formed at the same time because the reactions are reversible. The reactions would result in the pH value of solution in the range of 3 to 5. Though the reaction rate is slower compared to carbonates, the dissolution reactions within aluminosilicates are more likely to happen and yield more dissolved cations in the solution, especially for Anorthite according to the K_{eq} comparison. And the dissolution and precipitation could happen at the same time as well to reach an equilibrium. But the reprecipitation of aluminosilicates is not that easy to occur

compared to carbonates. Moreover, the acidity of the brine is sufficient to interact with aluminosilicate minerals which is the composition of clays and feldspars exist in sedimentary rocks, even after carbonate dissolution (Gaus, 2010). Therefore, these interactions could happen within one environment and could also have effect on each other in aspects of dissolution rate, overall amount of reaction and ion concentration.

Table 1. Mineral reactions with CO_2-Acidified Water

Mineral	Typical Reactions	Reaction Rate (mol·m^{-2}s^{-1})
Silicates	$SiO_{2(s)} + 2H_2O \Leftrightarrow H_4SiO_4 \Leftrightarrow H^+ + H_3SiO_4^- \Leftrightarrow H^+ + H_2SiO_4^{2-}$	1.26×10^{-14}
Aluminosilicates	Anorthite: $CaAl_2Si_2O_{8(s)} + 8H^+ \Leftrightarrow Ca^{2+} + 2Al^{3+} + 2H_4SiO_4$ $K_{eq} = 10^{21.7}$	Anorthite: 1.2×10^{-5}
		Oligiocalse: 1.2×10^{-8}
	Kaolinite: $Al_2Si_2O_5(OH)_{4(s)} + 6H^+ \Leftrightarrow 2Al^{3+} + 2H_4SiO_4 + H_2O$ $K_{eq} = 10^{3.8}$	Albite: 3.6×10^{-9}
		Kaolinite: 10^{-14} to 10^{-15}
Carbonates	$CaCO_{3(S)} + H^+ \Leftrightarrow Ca^{2+} + HCO_3^-$, $K_{eq} = 10^{1.85}$	Calcite: 1.6 to 3.2 ×10^{-5}
	$CaCO_{3(S)} + CO_2 + H_2O \Leftrightarrow Ca^{2+} + 2HCO_3^-$, $K_{eq} = 10^{-4.5}$	
	$CaCO_{3(S)} + H_2O \Leftrightarrow Ca^{2+} + HCO_3^- + OH^-$, $K_{eq} = 10^{-8.48}$	

After CO_2 is dissolved in the formation water and create carbonate ions, mineral carbonation happens. This interaction not only occur with calcium ions (Ca^{2+}) mentioned above to create calcite ($CaCO_3$), but also with other kinds of divalent metal cations such as Mg^{2+} and Fe^{2+}, forming carbonate minerals like magnesite ($MgCO_3$), dolomite ($CaMg(CO_3)_2$) and siderite ($FeCO_3$) (Snæbjörnsdóttir et al., 2014), and other kinds of more complicated interactions including alteration of feldspar and clay minerals (Gaus, 2010). Part of the interactions may happen in the reservoir conditions can be expressed by the following formulars:

$$Ca^{2+} + CO_3^{2-} \Leftrightarrow CaCO_3 \downarrow \quad \text{Eq. 7}$$

$$Mg^{2+} + CO_3^{2-} \Leftrightarrow MgCO_3 \downarrow \quad \text{Eq. 8}$$

$$Fe^{2+} + CO_3^{2-} \Leftrightarrow FeCO_3 \downarrow \quad \text{Eq. 9}$$

$$Ca^{2+} + Mg^{2+} + CO_3^{2-} \Leftrightarrow CaMg(CO_3)_2 \downarrow \quad \text{Eq. 10}$$

$$\underset{\text{Albite}}{NaAlSi_3O_8} + CO_2 + H_2O \Leftrightarrow \underset{\text{Dawsonite}}{NaAlCO_3(OH)_2} + \underset{\text{Chalcedony}}{3SiO_2} \quad \text{Eq. 11}$$

$$NaAlSi_3O_8 + CO_2 + 5.5H_2O \Leftrightarrow Na^+ + HCO_3^- + 2H_4SiO_4 + 0.5\underset{\text{Kaolinite}}{Al_2Si_2O_5(OH)_4} \quad \text{Eq. 12}$$

$$\underset{\text{Dolomite}}{CaMg(CO_3)_2} + 2H^+ \Leftrightarrow Ca^{2+} + Mg^{2+} + 2HCO_3^- \quad \text{Eq. 13}$$

$$\underset{\text{Chlorite}}{Fe_{2.5}Mg_{2.5}Al_2Si_3O_{10}(OH)_8} + 2.5\underset{\text{Calcite}}{CaCO_3} + 5CO_2 \Leftrightarrow 2.5\underset{\text{Siderite}}{FeCO_3} + 2.5\underset{\text{Dolomite}}{MgCa(CO_3)_2} + \underset{\text{Kaolinite}}{Al_2Si_2O_5(OH)_4} + \underset{\text{Chalcedony}}{SiO_2} + 2H_2O \quad \text{Eq. 14}$$

$$2\underset{\text{K-feldspar}}{KAlSi_3O_8} + 2H^+ + 9H_2O \Leftrightarrow 2K^+ + 4H_4SiO_4 + \underset{\text{Kaolinite}}{Al_2Si_2O_5(OH)_4} \quad \text{Eq. 15}$$

These interactions involving carbonate ions are also the principle of mineral trapping in the storage site. The properties and multiple phase flow were extensively studied by researchers all over the world, conceptually as well as experimentally. The formulars above have one thing in common that they occur in the existence of brine phase. However, the interaction between rock minerals and supercritical state CO_2 is being studied into. While so far it is widely considered that $scCO_2$ is chemical inert, there are some results from experimental works show that carbonation could happen without existence of brine (Jacques et al., n.d.; Regnault et al., 2005; Schaef et al., 2011). The results couldn't be simulated because current modelling methods rely on aqueous chemistry so they need to be confirmed through more experimental methods. More in-depth research is needed in $scCO_2$ interactions cause the near well environment will be dominated by $scCO_2$ during the injection stage (Gaus, 2010). Though carbonation is considered beneficial to sequestration of CO_2 in storage sites, mineral precipitation in reservoir pore space is considered one of the most commonly occurring formation damage mechanisms (Withjack et al., 2003) in some points of view. There are also other kinds of interactions may occur in the reservoirs not only with carbonate ions. For example, due to the existence of sulfate in formation water, dissolved calcium ions could also precipitate in the form of gypsum (or as anhydrite at depth). These sulfate minerals could cover the surface of the carbonates causing their passivation (García-Rios et al., 2013).

2.5. Conclusion

Before the implementation of a CCS project, it is crucial to confirm the storage capacity, injectivity and containment of the storage site in a long-term process for the reason of safety to both human beings and the environment due to the complexity in different types of reservoirs. The assessment should be conducted to master or predict how's the properties will be after CO_2 in injected into the storage site. The uncertainties mainly come from the interactions between injected CO_2, formation water and rock. For example, there is no evidence that geochemical interactions could cause or inhibit leakage under different conditions (Gaus, 2010). Experimental test is an important method to understand how the properties of the rock will change after exposure to CO_2 and the results are more intuitive and on a more detailed level compared to modeling. Besides, the database on impact of interactions between different phases needs to be enriched by more data support and the study results from experimental work could also contribute to model calibration in long-term time scales.

3. Methodology

3.1. Introduction

Stevns Klint chalk was chosen as analogue to chalk formations in the North Sea into this study to look into the feasibility of carbonate reservoirs, through the method of laboratory experiments. Properties related to the storage capacity and injectivity would be measured, compared and analyzed. The operation steps and theory of each measurement will be introduced and explained in this chapter.

3.2. Sample Preparations and Experimental Procedure

The chalk samples were collected from Stevns Klint, situated at the peninsula of Stevns, on the island of Sjælland (Zealand), Denmark and belong to latest Cretaceous (Maastrichtian) to Early Paleocene (Danian) age. The White Chalk, at the base of the cliff contains only scattered flint nodules, was used for this study. It corresponds in age approximately to the upper Tor to lower Ekofisk Formations in the North Sea chalk fields and has similar characteristics: 1) clean reservoir chalks with low content of clay and insoluble residue, 2) flow properties due to diagenesis had low impact on the outcrop chalk, 3) pore geometry deduced from capillary curve and pore distribution, 4) porosity/ permeability trend closely matches with high-porosity reservoir chalks. Therefore, it can be used as a field analogue to the chalk formations in the oil/gas reservoirs in the North Sea (Frykman et al., 2004).

9 samples, with diameter around 38 mm and length around 73.5 mm were taken into experiments after marking. 9 samples were divided into 3 groups: samples number 1 to 3 would interact with water and $scCO_2$, samples number 4 to 6 would interact with dry $scCO_2$, and samples number 12, 13 and 15 would be the control group.

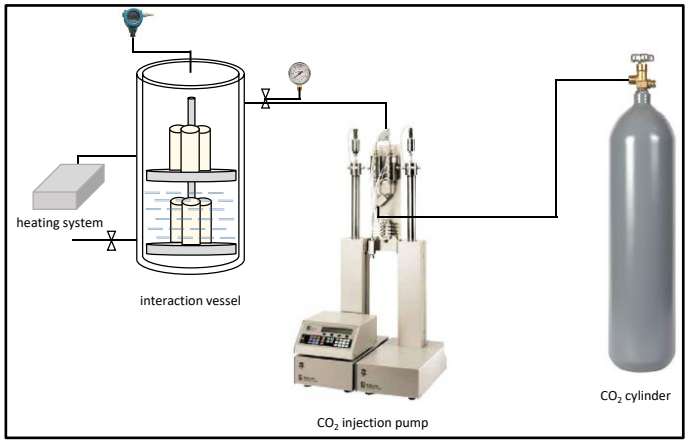

Figure 3. Schematic diagram of CO_2 exposure test.

The vessel used for fluid-rock interaction was a stainless-steel cylinder and can be sealed, pressurized and heated. There were two layers inside: on the bottom layer, the rocks numbering 1 to 3 were immerged into water for observing $scCO_2$-water-rock interaction and on the top layer, the rock samples numbering 4 to 6 were in gaseous environment before CO_2 injection and were for observation of $scCO_2$-rock interactions.

Before experiments, all the 9 samples were dried in the oven at temperature 70 °C for over 24 hours. Weight, diameter and length of them were measured after they were taken out from the oven and cooled down in a container isolated from air. Before put into the vessel, samples 1 to 3 were first vacuumed and then saturated with distilled water. After fully saturated and put onto the bottom layer, distilled water was poured into the cell over these samples for about 2 cm. Samples 4 to 6 were then put onto the top layer. Then the vessel was sealed, heated, and CO_2 was injected into it through the pump at the same time. For CO_2 needed to be in supercritical state in the cell during interaction, the pressure was set to 150 bar and temperature to 50 °C. While pressurizing and heating, the procedure was carried out gradually and slowly because as the temperature goes up, the volume of the gas inside will increase and that will lead to rise in pressure. After both of the pressure and temperature reached to the set values, valve of the pump for injecting CO_2 was closed to stop pressure rising but the heating system was on to keep the temperature at 50 °C. Pumping system was disconnected from the vessel after the pressure inside stabilized at 150 bar for over 12 hours. After interacting for 37 days, the vessel was depressurized by releasing CO_2 from "CO_2 inlet/ outlet" in Figure 4–left. Schematic diagram of CO_2 exposure test is shown in Figure 3.

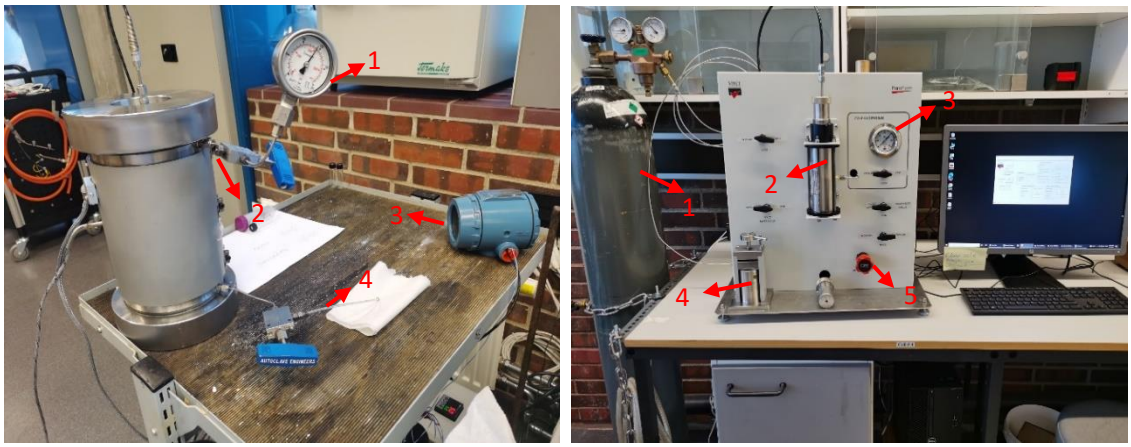

1. Pressure gauge
2. CO_2 inlet / outlet
3. Temperature sensor
4. Solution outlet

1. Nitrogen
2. Core holder
3. Confining pressure manometer
4. Matrix cup
5. Metering valve

Figure 4. CO_2 vessel (left) and porosimeter (right).

In order to understand what happened during the CO_2-fluid-chalk interaction and how the $scCO_2$ exposure process influenced the chalks, the following properties need to be measured before and after this interaction and compare the experimental results. It includes parameters of porosity, pore size distribution, permeability, specific surface area, thermostability, mineralogy and uniaxial compressive strength (UCS) of the chalk samples, and pH value and ion concentration of the solution samples from the CO_2 vessel.

3.3. Porosity

Porosity was measured through three different methods.

1. The first method was using apparatus *PoroPerm Prod AP-125-004-0* shown in Figure 4-right. Rock samples were put in the matrix cup (number 4) after drying. Noble gas nitrogen was used to inject into the matrix cup and the Boyle-Mariotte's Law was used to determine grain and pore volume:

$$\frac{P_{ref} \times V_{ref}}{T_{ref}} = \frac{P_{exp} \times V_{exp}}{T_{exp}} \quad \text{Eq. 16}$$

Within which P_{ref} and P_{exp} was initial pressure (about 100 psi) and final pressure (after matrix valve is opened, about 50 psi) respectively, V_{ref} referred to the volume of the tank(s) plus associated piping volume of the apparatus, $V_{exp} = V_{ref} + \left(V_{matrix} - V_{grain}\right)$ and temperatures were assumed constant during measurement, that is $T_{ref} = T_{exp}$. Then pore volume could be calculated:

$$V_{pore} = \frac{P_{ref}}{P_{exp}} \times V_{ref} - V_{dead} \quad \text{Eq. 17}$$

Where V_{dead} was V_{ref} plus the gas volume gathers the volume surrounding the core in the matrix cup. Then porosity could be calculated:

$$\phi = \frac{V_{pore}}{V_{core}} \quad \text{Eq. 18}$$

2. The second method was by using low field Nuclear Magnetic Resonance (NMR). The *MARAN-2* of 2MHz with 60mm diameter sample tube for rock core studies (Figure 5-left) was used for this test. Samples were dried in oven first, vacuumed and then fully saturated with distilled water before the tests. For each sample, a value of Phisize was given in the coming out data result. The application of low field pulsed NMR to analyze rock cores was based on the absorption of radiofrequency (RF) energy by the nuclear spins of the hydrogen nuclei (proton) in the presence of a fixed or static magnetic field. For each chalk,

two samples of solution fluid (with known and different weight) soaked through the rocks were tested, to get the relationship between Phisize and weight. Therefore, according to the Phisize values obtained from the rock samples, weight of the solution in each rock could be obtained. With tested density of each solution by density meter (Figure 5-right), volume of the solution inside the core could be calculated, that is the pore volume of each core sample. Finally, porosity could be calculated using Eq. 18.

Transverse relaxation time (T2) obtained from NMR test also gives valuable information about the physical environment of the fluid like size of pore where the fluid is located, so T2 distribution is a model of the pore size distribution in the core (Oxford Instruments, 2022). In this test, apparatus *MARAN-2* will give out the curve in y-axis of signal and x-axis of relaxation time (μs), within which a higher x-axis value represents for a bigger pore size and a higher y-axis value represents for a higher amount of a certain pore size.

1. Sample tube
2. Rock samples
3. Solution samples

Figure 5. Nuclear Magnetic Resonance (NMR) (left) and density meter (right).

3. The third method was through saturating the chalk samples, together with tested chalk density and saturating fluid density to calculate the porosity. After drying each sample in the oven, the weight (W_d) of them need to be measured after cooling down. After fully saturated with distilled water, measured the weight (W_b) of them again. Density of chalk ρ_{rock} can be measured using apparatus in Figure 4–right, density of fluid ρ_{fluid} can be measured by density meter in Figure 5-right. Porosity then could be calculated by equation:

$$\phi = \frac{V_b - V_d}{V_b} \qquad \text{Eq. 19}$$

where,

$$V_d = \frac{W_d}{\rho_{rock}} \quad \text{Eq. 20}$$

is the matrix volume of rock sample, and

$$V_b = \frac{W_d}{\rho_{rock}} + \frac{W_b - W_d}{\rho_{fluid}} \quad \text{Eq. 21}$$

is the bulk volume.

These three methods were done for all the 9 chalk samples.

3.4. Permeability

PoroPerm Prod AP-125-004-0, same with the apparatus used in the first method for measuring porosity (Figure 4-right) was used for permeability measurement. Gas nitrogen was injected through the rock samples with a flow rate Q and a pressure P. The calculation of permeability was derived from Darcy's law which for liquids under steady state conditions of laminar flow:

$$k = \frac{\mu Q L}{A \Delta P} \quad \text{Eq. 22}$$

The equation:

$$k_g = \frac{\mu P_b Q_b L}{A \Delta P P_m} \quad \text{Eq. 23}$$

is used to calculate core permeability to nitrogen, under laminar flow conditions.

where: P_b is barometric or atmospheric pressure,

Q_b is atmospheric gas flow rate at P_b,

P_m is mean core gas pressure.

Klinkenberg calibration was required to acquire the permeability equal to the value in formation condition. For each rock, permeability to gas was measured 4 times by controlling metering valve and then a trend line with y-axis of gas permeability and x-axis of $1/P_{mean}$ was derived. The intercept of the trend line is then the permeability in formation condition according to standard Klinkenberg equation:

$$k_g = k_L \cdot \left(1 + \frac{b}{P_{mean}}\right) \quad \text{Eq. 24}$$

where: k_L is permeability to liquid,

b is gas slippage factor,

P_{mean} is core mean pressure.

The tests were operated under flow rate control to reach the stabilization, the flow rate gradient of 5, 10, 15, 20 and 30 cc/min was done for each rock. This permeability measurement was done for all the 9 samples.

3.5. Specific Surface Area

Specific surface area of a porous material is the interstitial surface area of pores per unit of bulk volume or solid volume of the porous material (Rabbani et al., 2014). It is an essential petrophysical property to characterize natural reservoirs through means like complex electrical properties, fluid dynamics and chemical reactions between pore fluids and matrix minerals (Specific Surface Area of Porous Rocks: An Integrated Approach by Combination of BET and Micro-CT Imaging - NASA/ADS, n.d.), and is a critical parameter to fluid permeability of a porous media (Rabbani et al., 2014). The BET (Brunauer, Emmett and Teller) theory here was used to evaluate the surface area by looking into the physical adsorption of gas molecules on a solid surface and come out with a specific surface area result, in the unit of m^2/g. The probing gas chosen should not interact with the adsorptive used for quantifying specific surface area (BET Theory - Wikipedia, n.d.). This whole process is shown in Figure 6-a).

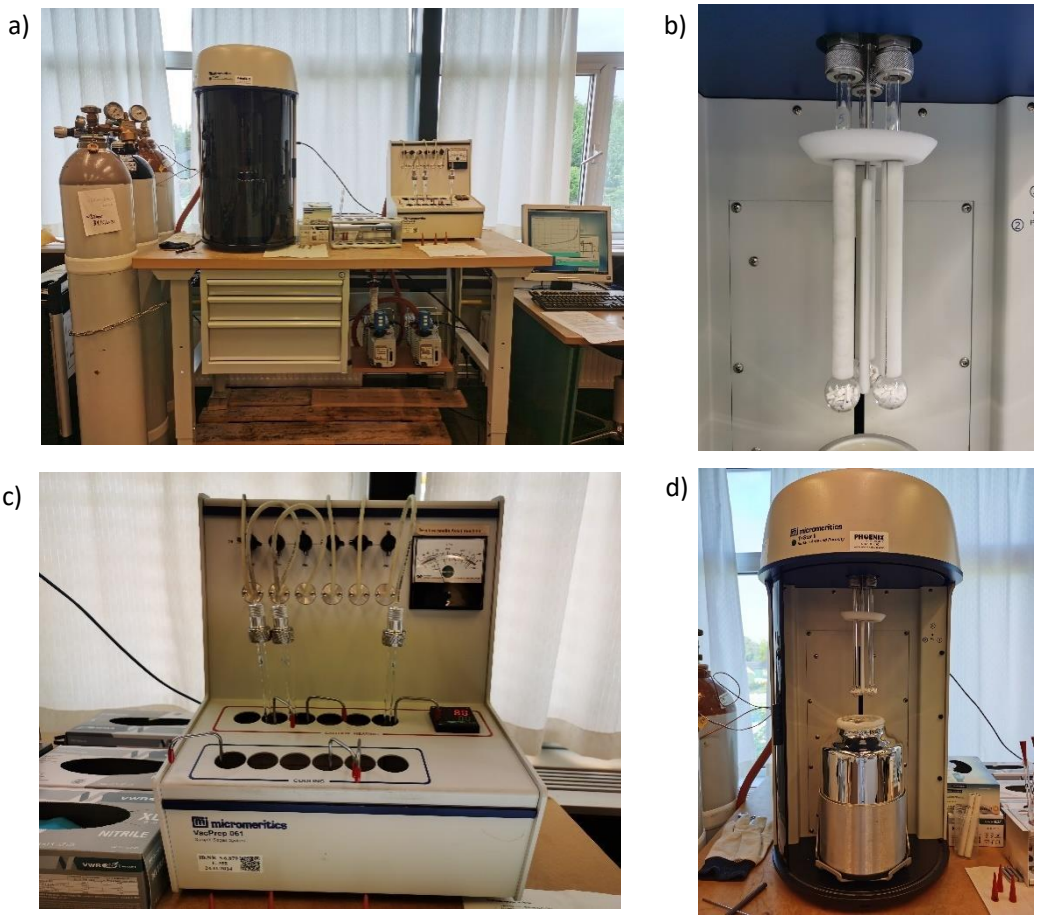

Figure 6. Complete process for BET analysis (a), samples prepared for BET (b), sample degas system (c), and TriStar II 3020 for sample analysis (d).

The rock samples of 2 to 3 grams are needed for each core. They were prepared in small pieces in glass tubes shown in Figure 6-b) and the dust or powder on the samples need to be avoided since they would increase the surface area. Before analysis, the attached impurities on the sample surface needed to be removed, by increasing the temperature of the samples to 80°C and at the same time vacuum or injecting a continuous flow of inert gas. This process is called degassing (BET Specific Surface Area - Particle Technology Labs, n.d.) and conducted in the apparatus in Figure 6-c). Degassing time was set 4 hours and the pressure needed to be below 100 mTorr after degassing was complete. The weight of the empty glass tube (together with stopper) and after degassing was measured to get the weight of the samples. The physical adsorption of nitrogen onto the surface of the chalk samples at cryogenic temperatures was then used to measure the surface area of the samples (the liquid nitrogen was used). Apparatus TriStar II 3020 in Figure 6-d) was used for this test. Results of specific surface area and pore distribution could be obtained after BET analysis.

3.6. Thermostability

Thermostability, as another important quality of material, is used to evaluate how well the material can resist irreversible change in its chemical or physical structure (Wikipedia, 2021). This quality of chalk samples before and after exposure to $scCO_2$ need to be tested. Thermogravimetric analysis (TGA) was the method for this test and apparatus *TGA/DSC 3+* (Figure 7-left) was used. In this test, mass of the material was continuously measured when the temperature increased over time. The start temperature and end temperature were set at 25 °C and 800 °C respectively, heating rate was 10 K/min, method gas was nitrogen at a flow rate of 20 ml/min and the experiments were performed in an alumina crucible (70 µL). For each chalk sample, 10 mg ($\pm$0.02 mg) chalk powder was put in alumina crucible each time, in order to eliminate possible interference factors caused by inconsistent weight. The whole process lasted at temperature rising from 25 °C up to 800 °C and stabilized at the peak temperature for another 1 hr. This test was done for all 9 chalk samples in sequence.

TGA test can give out the result of weight changes of chalk samples in relationship with temperature or time, in which the decomposition or composition process can be observed due to mass loss or increasement. The weight can increase or decrease in TGA. The mechanisms of weight loss can be decomposition (the breaking apart of chemical bonds), evaporation (the loss of volatiles as a result of increased temperature), reduction (interaction of the mineral to a reducing atmosphere like hydrogen and ammonia) or desorption. And for weight gain, the mechanism can be kinetic processes of oxidation (the reaction to an oxidizing environment) or absorption / adsorption.

And for Differential Scanning Calorimetry (DSC) test, it's a thermoanalytical technique measuring the difference in the quantity of heat needed to raise the temperature of a sample and an inert reference. It is determined as a function of

temperature and time (Höhne et al., 1983). Therefore, an empty alumina crucible is also needed to be measured in the apparatus using the same method as a reference. The quantitative and qualitative information about physical and chemical changes which endothermic or exothermic processes in heat capacity are included can be looked into (Hepzi et al., 2016). Through DSC-TGA, the transition temperature, heats of fusion and reactions, melting and boiling points, decomposition kinetics of materials, lifetime of products, composition of multi-component systems, thermostability of materials, etc. can be obtained (Banerjee, n.d.).

Figure 7. TGA/DSC 3+ (left) for TGA test and Optical Emission Spectrometer Optima 4300 DV (right) for ICP test.

3.7. Mineralogy

Mineralogy was observed through the following two different methods.

1. Scanning Electron Microscopy (SEM) & Energy Dispersion Spectrum (EDS).

   Before observation, the rock samples were cut into small pieces and covered by copper layer to make it conductive. The bottom of small pieces should be as flat as possible, for being more conductive lying on the observation plate. Because chalk is non-conductive, then with chosen pieces on the plate, a layer of copper with thickness of 40 nm was used to cover over the chalk pieces to make it conductive for following observations. The apparatus used for covering copper is shown in Figure 8-left. The apparatus for SEM-EDS test is shown in Figure 8-right. The surface texture and morphology of the rock were observed from SEM test and images were taken in different magnifications. After SEM test, EDS test was done for mineral composition analysis of each rock sample. The SEM-EDS test observation could show clear signs of pore structure and mineralogical changes of rock samples.

2. X-ray diffraction (XRD)

   X-ray diffraction analysis is a technique used in material science to determine the crystallographic structure of a material. It works by irradiating the material with

incident X-rays and then measuring the intensities and scattering angles of the X-rays that scattered by the material. The result of XRD is shown in the relationship between intensity of the scattered X-rays and scattering angle. And through the analysis of the location, in angle and the intensities of scattered intensity peaks, the structure of the material can be determined. XRD is a standard method for determining the presence (or absence) of crystallographic order in materials. And at the same time, it is often used to explore other structural information like determine whether the material is amorphous or composite material, the grain size of the material, and the degree of the texture in material (X-Ray Diffraction for Determining Atomic and Molecular Structure | Materials Engineering | JoVE, n.d.). The test here was conducted to compare the mineral alteration triggered from rock-scCO_2 interaction.

Bruker D8 Advance Eco diffractometer equipped with a Lynxeye detector (Cu-Kα radiation, 40 kV voltage, 25 mA current) was used in this XRD test (Figure 9). Measuring conditions were set to analysis from 5-90 degrees using a 0.6 mm divergence slit, with a measuring time of 1 degree per minute while rotating the sample continuously during measurement. Phase identification and data visualization were performed with the software Diffrac.Eva, combined with the PDF-4+ database from the International Centre for Diffraction Data (ICDD).

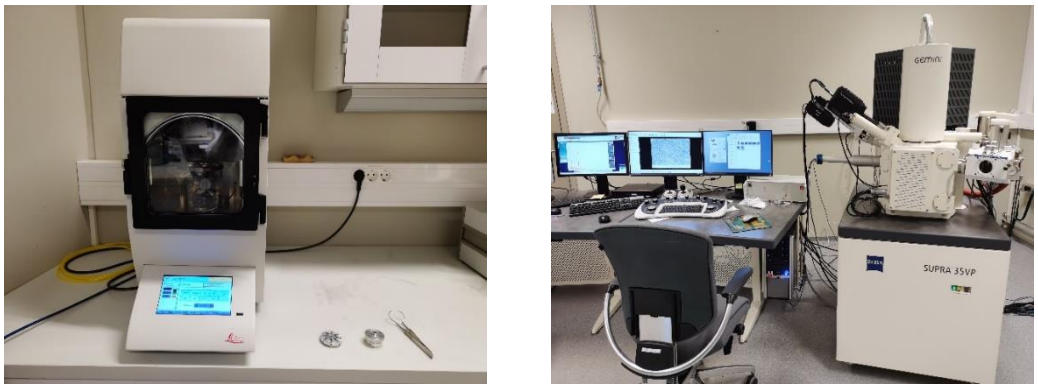

Figure 8. EM ACE600 (left) for coating rock samples with copper layer and SUPRA-35VP (right) for SEM & EDS analysis.

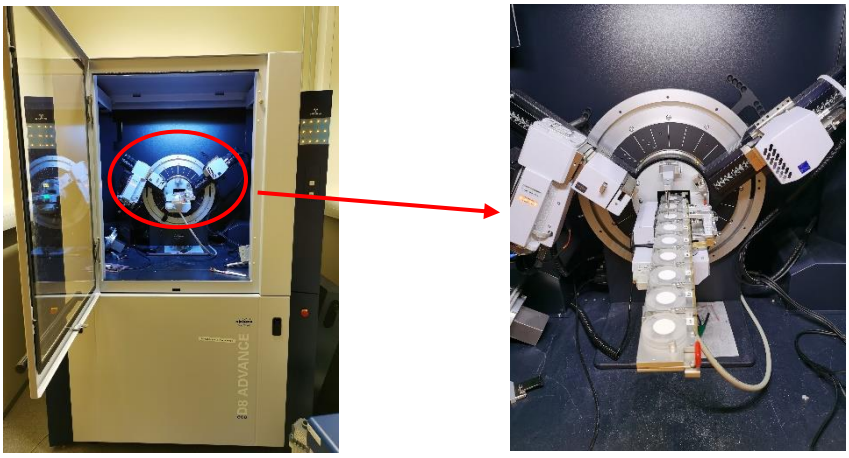

Figure 9. Bruker D8 Advance Eco diffractometer sued for XRD analysis.

3.8. pH Value and Ion Concentration

After CO_2 was injected into the cell, it may dissolve in water, creating carbonic acid and then decrease the PH value of the fluid. Dissolution may occur among the rocks numbering 1 to 3 immersed in the solution. Analysis of the solution at different time stages could help to discover what kind of minerals in chalk could be dissolved by carbonic acid, its dissolution velocity and also the variation trend over time under certain conditions including pressure and temperature. Solution samples were taken 5 times in the 8^{th}, 13^{th}, 27^{th}, 34^{th} and 37^{th} day of interaction, numbering sample 1 to 5 respectively. The volume was about 15 ml each time. These samples were taken from solution outlet (Figure 4–left) during interaction, along with distilled water and the solution sample which was taken after rocks immerged in distilled water before CO_2 injection (numbered sample 0) as control samples were sent to determine pH value. The solution samples need to be kept not being contaminated during pH test so that they could be sent to analysis ion concentration afterwards. pH value could give the information whether interactions were in progress inside the vessel without taking the samples out and ICP analysis could give more detailed information about what kind of dissolution or precipitation happened at each step according to the ion concentration. Every time after solution samples were taken from the interaction vessel, CO_2 inlet should be reconnected to CO_2-injection pump and repressurize CO_2 vessel back to 150 bar to keep the interaction environment at the same pressure condition.

Ion concentration was determined by Inductively Coupled Plasma (ICP) and apparatus *Optical Emission Spectrometer Optima 4300 DV* (Figure 7-right) was used for ICP test. For all 7 solution samples (including distilled water), they were diluted into two different ion concentration solutions before determination. One was a 10 ml solution sample with nitric acid (HNO_3) concentration of 5%, diluted by 65% HNO_3 solution. That is, 9.231 ml of original solution sample mix with 0.769 ml 65% HNO_3 solution. The other one was also a 10 ml solution, made by mixing 1 ml original solution sample with 9 ml 5% HNO_3 solution. The dilution factors were 1.083 and 10

respectively. In this test, ions including potassium (K^+), sodium (Na^+), calcium (Ca^{2+}), magnesium (Mg^{2+}), aluminum (Al^{3+}), silicon (Si^{4+}), etc. were determined. From observing variation in ion concentration, the interactions including dissolution and precipitation of the minerals could be looked into.

3.9. Uniaxial Compressive Strength (UCS)

Uniaxial Compressive Strength (UCS) stands for the maximum axial compressive stress that a sample can withstand before failing under zero confining stress. It's one of the most essential mechanical characteristics of rocks for determining the structural integrity of constructions under load. Measurement of the quality of the rock is extremely important for safety of the CO_2 storage site. The unconfined compression test can be used to measure UCS. The core samples used for UCS test need to follow some restrictions. The diameter should be at least 47 mm and the length-to-diameter ratio of the sample should be between 2 and 2.5. The sample's ends should be leveled within a 0.02 millimeters tolerance and shouldn't depart from perpendicularity by more than 0.06 degrees. The cylindrical surfaces need to be flat and smooth (Unconfined Compression Test | Geoengineer.Org, n.d.). The results of the UCS tests would be presented in the curves of Load (kN) in y-axis and Crosshead (mm) in x-axis in the system. The UCS could be obtained from the peak value of the curve (divided by the cross-sectional area of each core sample).

In the UCS tests conducted in this study, the samples were all dried in the oven of same moisture condition for the test. For the dimensions, they didn't meet the diameter condition required and the length was cut to fulfill the NMR measurement. But all the samples were about the similar diameter and length so the compared results could still illustrate whether the exposure to CO_2 weakened or enhanced the mechanical properties after exposed to $scCO_2$. The apparatus *MTS Criterion C45.105 load frame* used for these measurements is shown in Figure 10. Test rate was set at 0.05 mm/min. Axial load was continuously increased on the chalk samples until peak load and failure were obtained.

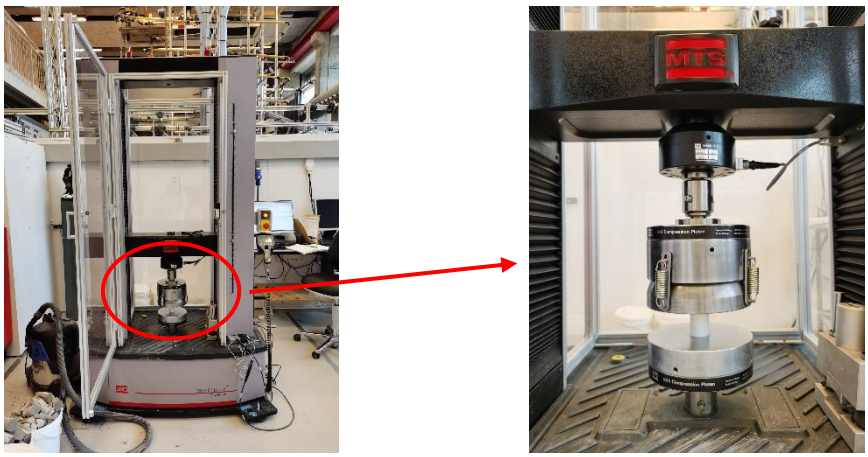

Figure 10. MTS Criterion C45.105 load frame for UCS test.

3.10. Conclusion

Through each experimental measurement of the rocks and the solution samples, the properties of the chalk after exposure to $scCO_2$ would be obtained. And the storage capacity and injectivity would be deducted after discussion and analysis of these data. Then it could come to a conclusion whether chalk would be a feasible storage site for CO_2 according to these experimental data. The results and discussions would be presented in the next chapter.

4. Results and Discussions

4.1. Introduction

After interaction for 37 days, the rocks were taken out from the CO_2 vessel. Figure 11 shows the images of chalks after exposure to $scCO_2$ in condition of with and without water presence. There was difference in color between two groups when taken out (Figure 11-left) but after being dried in oven for over 24 hours (Figure 11-right), there were no significant differences visually observed. In order to get a further understanding, in depth analysis are needed to evaluate the changes in the pore structure. The results of each measurement will be presented in this chapter.

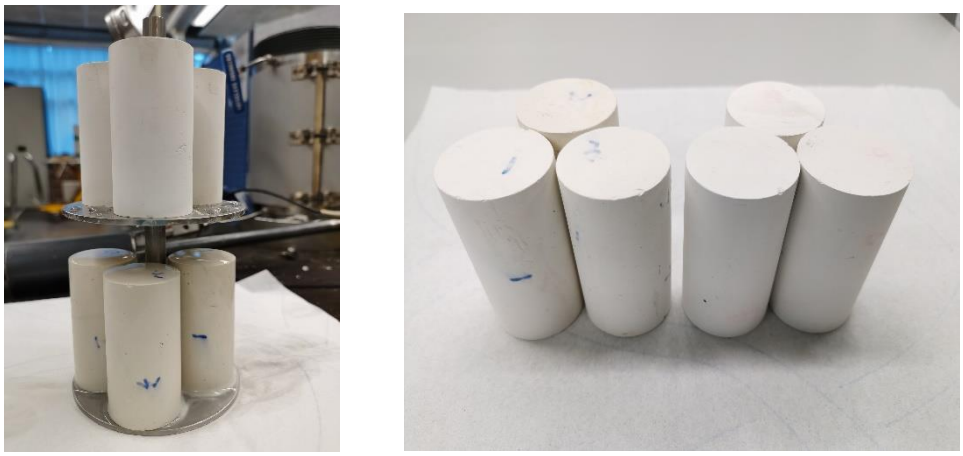

Figure 11. Chalk samples taken from CO_2 vessel (left) and after dried for over 24 hours (right).

4.2. pH Value

pH value of the solution was obtained before chalk samples were taken out from the CO2 vessel during exposure test. It was the first serious of values obtained before other parameters measurement. The results are shown in Figure 12. It started from 9.44, at which time number 1 to 3 chalk samples were immerged in distilled water and before CO2 injection. This value is consistent with the study result that at 20 °C, the highest pH value of the solution could reach to highest value of 9.7 after calcium carbonate is dissolved and decrease with decreasing temperature (L. Sun, n.d.). It started to decrease after CO2 was injected into the vessel. From the 13th day of interaction, pH value kept in the range of 6.5 to 6.7 until the end of the exposure test. Through the pH value variation, it could be inferred that scCO2 dissolved in the solution interacted with other ions dissolved, which triggered pH value decrease and there should be ion concentration variation at the same time or new ions could be detected through the following ICP test.

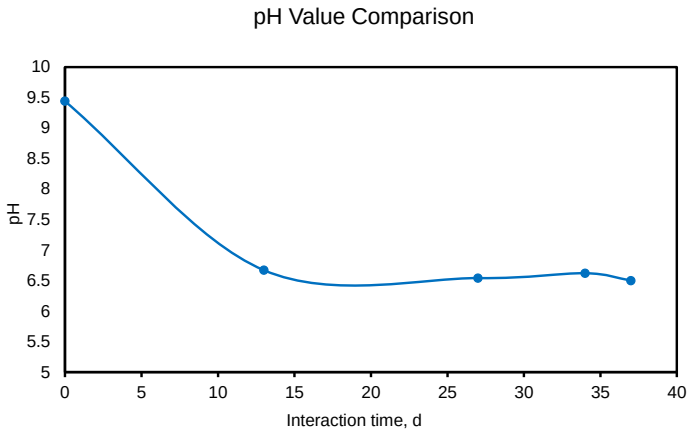

Figure 12. Variation in pH value.

4.3. Porosity

Porosity results through 3 methods for all 9 samples are shown in Figure 13. The left is the comparison between intact ones in red and $scCO_2$ group in green and the right is between intact and water+$scCO_2$ group in blue. Detailed data is presented in Table 3. Before interaction, porosity was in the range of 46.5% to 56.5%. After interaction, the range of the porosity was between 46% and 58.5% for $scCO_2$ group and between 45% and 53% for water+$scCO_2$ group. Comparing this data, porosity range of $scCO_2$ group was widened and water+$scCO_2$ group was narrowed and at the same time decreased more obviously compared to the other group.

From Figure 13, it is observed that within each rock sample, NMR gave the highest porosity value within 3 methods except sample 1 and the other two methods gave similar values. Comparing intact group (sample 12, 13, 15) and $scCO_2$ group (sample 4 to 6): through method 1 and method 3, porosity showed a slightly increase after interaction but through method 2, the value showed a slightly decrease. These changes are more straightforward when comparing their average value of each group from Table 3 and the increase or decrease percentage were 1.35%, -0.77% and 1.96% through each method. But considering heterogeneity of the rock, it's difficult to draw the conclusion that porosity was increased or decreased after rock-$scCO_2$ interaction because of the inconsistent results and the tiny differences. But the situation is clearer when comparing intact group (sample 12, 13, 15) and water-$scCO_2$ group (sample 1 to 3). Through all the 3 methods, the porosity all showed a decreasing trend after interaction. The variation percentage of porosity were -0.78%, -9.27% and -0.98% through each method when comparing the average porosity value of each group.

Various errors may occur during the experiment that could result in different values through different methods. In method 1 of using porosimeter, the weight, diameter and length of each sample should be typed into the apparatus in Figure 4-right and the porosity is calculated based on these parameters. At the same time the rock samples were not perfect cylinders so they don't have a fixed diameter and length in all directions and these two values were measured by vernier caliper, which could

also cause errors during measurement. In method 2 of NMR, this analysis was done after core samples were saturated with water. Therefore, the degree of saturation (fully saturated or not) and how to deal with the water on surface of each rock after saturation, matter the Phisize detected by NMR, which related to the amount of solution in the sample and affect porosity measurement ultimately. And in method 3 of calculation, rock density in Table 2 for calculation came from porosimeter in Figure 4-right, with errors mentioned in method 1. And errors created during saturation process mentioned in method 2 may also be another reason here. Combining the principles of each apparatus, the errors may occur within these three methods and heterogeneity of chalk itself, it's understandable that to even the same core, porosity had different results through various methods or from different cores in one group. Therefore, it's necessary to have a group of samples in each condition to eliminate avoidable errors. Though in the presence of errors, the variation of porosity after interaction could still be observed.

Table 2. Rock sample density measured by porosimeter and tested density of solution after rock saturated with distilled water measured by density meter.

sample		rock density, g/cm3	solution density, g/cm3
water+scCO2	1	2.7235	0.99823
	2	2.7195	0.99827
	3	2.7250	0.99821
scCO2	4	2.7185	0.99823
	5	2.7135	0.99827
	6	2.7100	0.99823
intact	12	2.7255	0.99825
	13	2.7375	0.99821
	15	2.7520	0.99820

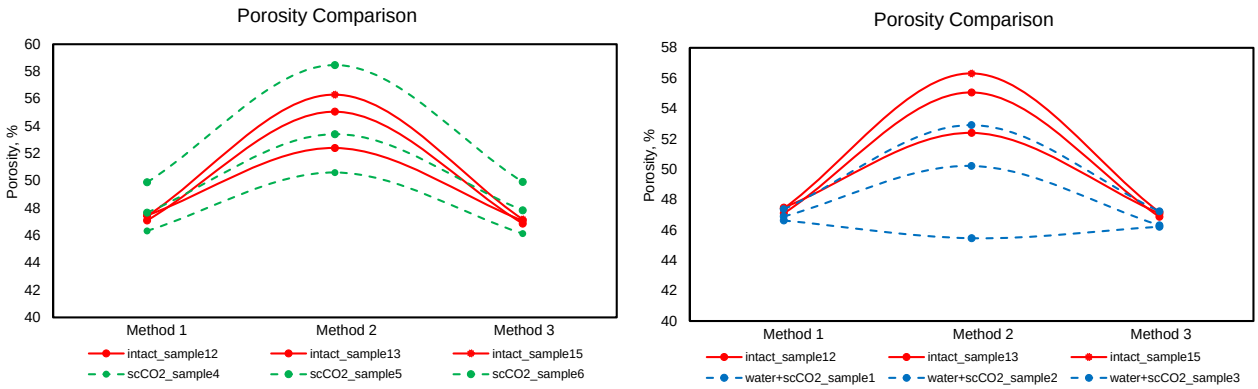

Figure 13. Porosity comparison between intact and $scCO_2$ group (left), and intact and water+$scCO_2$ group (right).

Table 3. Porosity values of 9 chalk samples measured through 3 different methods.

Sample	Method	1_Porosimeter	2_NMR	3_Equation
intact	12	47.47	52.40	47.08
	13	47.10	55.06	46.87
	15	47.42	56.31	47.17
	average	**47.33**	**54.59**	**47.04**
scCO2	4	46.34	50.61	46.13
	5	47.68	53.42	47.84
	6	49.90	58.47	49.92
	average	**47.97**	**54.17**	**47.96**
water+scCO2	1	46.63	45.45	46.21
	2	46.89	50.22	46.30
	3	47.37	52.91	47.23
	average	**46.96**	**49.53**	**46.58**

4.4. Pore Size Distribution

Results of pore distribution were obtained through 2 methods: NMR measurement and BET method. Result from NMR is shown in Figure 14. According to the curves presented, the peaks of $scCO_2$ group and water+$scCO_2$ group both showed a shift to left compared to intact group. Higher relaxation time in x-axis represents for bigger pore size. That is, the overall pore size of the rocks for both $scCO_2$ and water+$scCO_2$ group declined after interaction. This result is consistent with porosity declination for both of the groups through NMR method. Result from BET method is shown in Figure 15. The data is from BJH method during adsorption process. Though the variation in the result through BET method is not as clear as in the result through NMR method, a shift to the left can still be distinguished.

Parameters in pore space are critical in aspect of storage capacity, representing for how much CO_2 could be stored in the storage site. Though porosity and pore size had a declination after interact with water and $scCO_2$, it still showed a relatively high porosity of 46% to 50% compared to average porosity in sandstone of 14.8% (Nolan, n.d.). Based on porosity and pore size tests, chalk shows a good capacity for CO_2 storage. But whether chalk is suitable for CO_2 storage is not only depends on storage capacity. The following tests for other properties determination are also crucial.

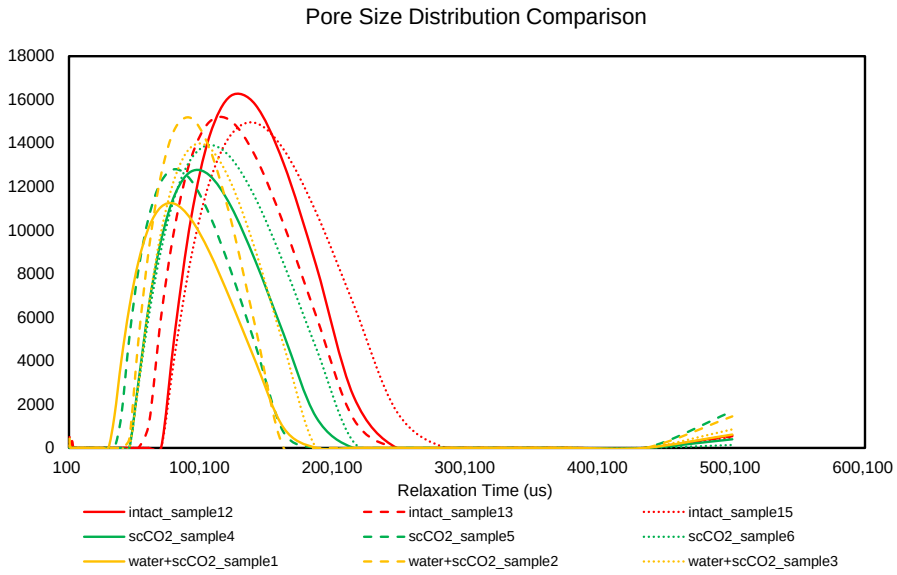

Figure 14. Pore size distribution comparison from NMR.

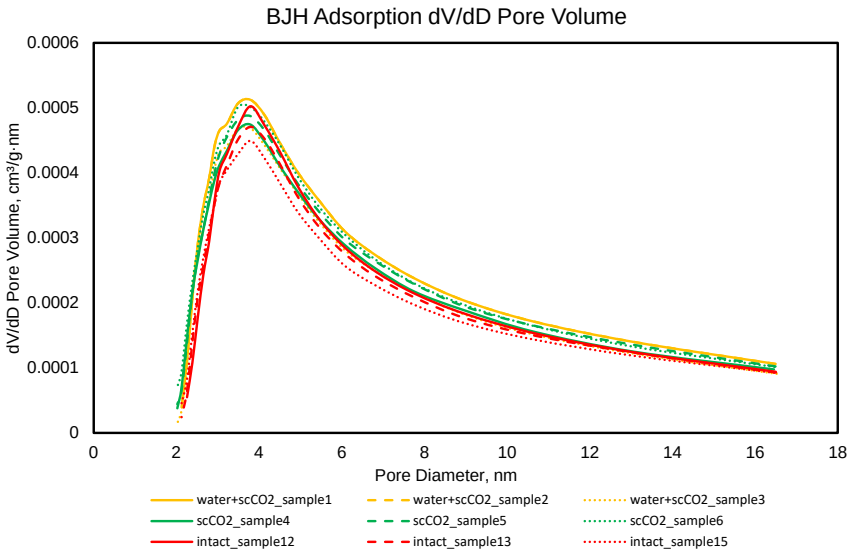

Figure 15. Pore size distribution comparison from BET.

4.5. Permeability

Permeability results through injecting nitrogen in 5 different flows rates are shown in Figure 16 and data is presented in Table 4.

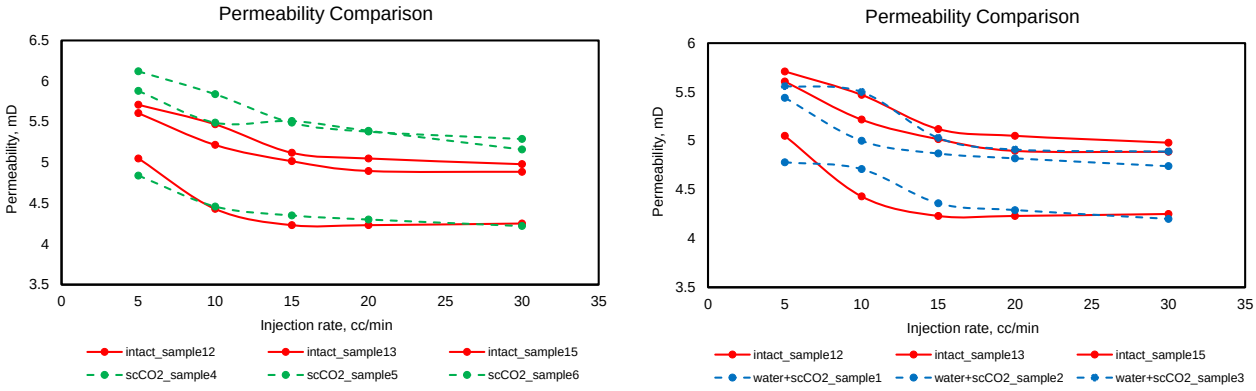

Figure 16. Permeability comparison between intact and $scCO_2$ group (left), and intact and water+$scCO_2$ group (right).

Table 4. Permeability values of 9 chalk samples measured by 5 different nitrogen injection rates.

sample \ rate(cc/min)		5	10	15	20	30
intact	12	5.71	5.47	5.12	5.05	4.98
	13	5.05	4.43	4.23	4.23	4.25
	15	6.06	5.75	5.7	5.41	5.43
	average	**5.61**	**5.22**	**5.02**	**4.90**	**4.89**
scCO2	4	5.88	5.49	5.51	5.39	5.16
	5	4.84	4.46	4.35	4.3	4.22
	6	6.12	5.84	5.49	5.38	5.29
	average	**5.61**	**5.26**	**5.12**	**5.02**	**4.89**
water+scCO2	1	4.78	4.71	4.36	4.29	4.2
	2	5.44	5	4.87	4.82	4.74
	3	5.56	5.5	5.03	4.91	4.89
	average	**5.26**	**5.07**	**4.75**	**4.67**	**4.61**

Comparing the permeability results between intact group and $scCO_2$ group from curves in Figure 16-left, the distribution was widened slightly upwards. And from the data results in Table 4 of average value in each group using different injection rates, permeability was equal to the intact group at the maximum and minimum injection rate, and showed increased values at injection rate of 10, 15 and 20 cc/min. Comparing water+$scCO_2$ and intact group in Figure 16-right, the distribution was narrowed slightly a little bit. It's easy to conclude that permeability decreased after chalk samples were exposed to wet $scCO_2$. It's more obvious through the average results presented in Table 4. The average permeability decreased at all the 5 different injection rates, ranging from 2.81% to 6.18% and had the average decrease percentage of 4.89%.

Comparing the permeability at 5 different injection rates of each sample, all the 9 samples gave a decrease trend as the injection rate increases. This trend may because of when it was at low injection rate, the nitrogen flow cleaned the particles in the pore space towards the injection direction but due to the low permeability, these particles couldn't find a way going through the chalk sample and stuck on their way out. And these stuck particles then had the high possibility of block the pore

throat and decrease permeability.

In permeability test, the errors from diameter and length measurement could also influence the results as in method 1 of porosity measurement. But the trend of permeability variation could still be observed. The reason for porosity and permeability declination between water+scCO$_2$ and intact group could be found in the following tests.

4.6. Specific Surface Area

Specific surface area result through BET method is illustrated in Figure 17 below. It is clear to see that after both of the interactions, specific surface area increased and it is more obvious to the water+scCO$_2$ group.

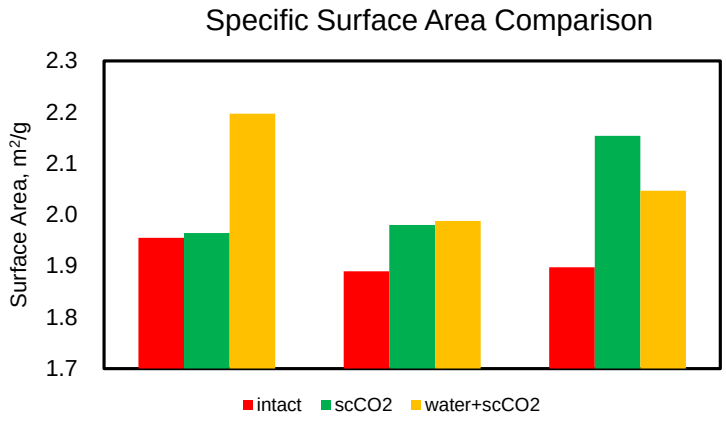

Figure 17. Permeability comparison between rock samples before (red) and after (green and yellow) interactions.

Specific surface area is affected by different sample features including micro fractures, pore space cementation and existence of clay minerals (Specific Surface Area of Porous Rocks: An Integrated Approach by Combination of BET and Micro-CT Imaging - NASA/ADS, n.d.). To the scCO$_2$ group, the pore structure was changed after interaction according to the porosity, permeability and pore size distribution results. And the variation in specific surface area added more proof to that chalk could interact with scCO$_2$ and change its pore structure. For the water+scCO$_2$ group, the specific surface area increased more could be result that the interaction happened in the solution was more active compared to the one with scCO$_2$. The relationship between specific surface area and permeability can be described by the equation (Costa, 2006):

$$k = \frac{C_p \phi^3}{(1-\phi)^2} \times \frac{1}{S^2} \qquad \text{Eq. 25}$$

where C_p is a constant related to the shape of the pores, ϕ is the porosity, and S is the specific surface area. According to the equation, if the specific surface area increases, permeability will decrease. And this is in accordance with this study that after interaction with water and $scCO_2$, permeability decreased and specific surface area increased. But there is no specific relationship between pore parameters and specific surface area shown here that samples with higher porosity or pore size get a certain higher or lower specific surface area.

4.7. Ion Concentration

Results of ion concentration variation of solution from ICP test is shown in Table 5. Sample 0 is the solution taken after chalk samples immerged into distilled water before CO_2 injection and sample 1 to 6 were taken in turn during interaction process until the end of exposure test. The sample of distilled water was also measured and values in Table 5 are the results that exclude the effect from distilled water. Ions including calcium (Ca), sodium (Na), magnesium (Mg), potassium (K), silicon (Si), etc. could be tested in the solution. Ca ions had the most significant change during interaction among all the ions. The content of Ca greatly increased after CO_2 was injected into the vessel but then decreased during the following interaction process. The trend was the same with K and Zn ions but the concentrations were much lower compared to Ca ions. As to Si ions, the content steadily increased within interaction time from its initial value. The contents of Na, Mg and Sr ions merely showed slight fluctuations with no significant changes. And for the ions like Al, Ba, Mn, etc., the contents were very low and could hardly be tested. In this process, Ca^{2+} created by dissolution of calcite, and CO_3^{2-} created by dissolution of CO_2 in the solution triggered the precipitation of calcium carbonate in the pore space of the samples and also at the bottom of the vessel inside. It should be mentioned that after chalk samples immerged in distilled water, there was observed a layer of dust on the surface of solution, which could be mobile fines from rock samples. Some of these dusts dissolved in the distilled water and contributed to the Ca ions in sample 0. After CO_2 injection, more dusts were then dissolved by acidification and performed as ions in the solution samples.

The ICP result is the explanation of porosity, permeability, pore size distribution and specific surface area variation after interaction with water and $scCO_2$. After $CaCO_3$ dissolved into the solution, making the Ca ion concentration increased to the highest value recorded at 1037 mg/L, it then decreased to 226 mg/L at the end of the exposure test. The dissolution of CO_2 leaded to significant variation in solution through interactions of CO_2 with ions in solution and rock minerals. That means, Ca ions reprecipitated with anions in the solution after dissolution process and there is part of the sediment settled at the bottom of the CO_2 vessel that could be observed after exposure test, and at the same time there must be part of the compound settled in the pore space of the chalk samples. The compound in the pore space decreased the pore space and porosity, and the permeability decreased when they stuck at the pore throat. Because the specific surface area of the dusts is higher

compared to the core samples, this precipitation of calcium ions could increase the specific surface area. The minerals created during precipitation process would be studied more in the following mineral analysis of SEM & EDS and XRD measurements.

Table 5. Ion concentration comparison from ICP test.

Element, mg/L / Sample	Na	Ca	Mg	Si	Al	K	Ba	Mn	Zn	Sr
0	0.42	4.2	0.03	<0,01	<0,01	1.9	<0,01	<0,01	<0,02	0.02
1	15.4	1037	8.6	5.8	0.02	2.3	0.3	0.0	0.8	6.5
2	15.5	1000	8.7	7.1	0.01	14.4	0.3	0.0	0.8	6.5
3	15.4	1014	9.4	10.0	0.02	10.0	0.3	0.0	0.8	6.9
4	15.8	951	9.4	10.9	0.02	8.5	0.3	0.0	0.5	6.6
5	15.9	226	8.7	11.6	0.01	2.5	0.1	<0,01	0.2	4.6

4.8. Thermostability

TGA result is shown in Figure 18 with weight percentage in y-axis and temperature in x-axis. Comparing the $scCO_2$ (green) and intact (red) group, though the average temperature of complete decomposition still showed a declination of 4 °C after interaction, the distribution of green curves ranged from 774 °C to 782 °C. It's difficult to draw the accurate conclusion of whether the complete burning temperature of chalk samples was decreased or not after interact with dry $scCO_2$. But when comparing the water+$scCO_2$ (orange) and intact (red) group, there's a shift to left after interacting with $scCO_2$ in the presence of water. That is, the complete decomposition temperature of rocks after interacting with water and $scCO_2$ decreased from 782 °C to 777 °C, having 5 °C of declination. In Figure 18, the curves started to decompose at a low rate and went more quickly as the temperature went higher. From previous research, thermal decomposition (or called calcination) of calcite takes place between temperature of 700 °C and 800 °C (Karunadasa et al., 2019). And in this test, the result showed that at the temperature of around 660 °C, the weight of the sample started to decline and that is also the point calcium oxide and carbon dioxide started to create. The end of the decreasing point at around 780 °C is the completion of decomposition. When it comes to the difference of completion temperature of decomposition within intact and water+$scCO_2$ ones, it may could be explained by study result from Karunadasa et al. that CO_2 could catalyze the conversion of trigonal $CaCO_3$ (calcite) to cubic CaO, which made the transition completed at an apparently low temperature.

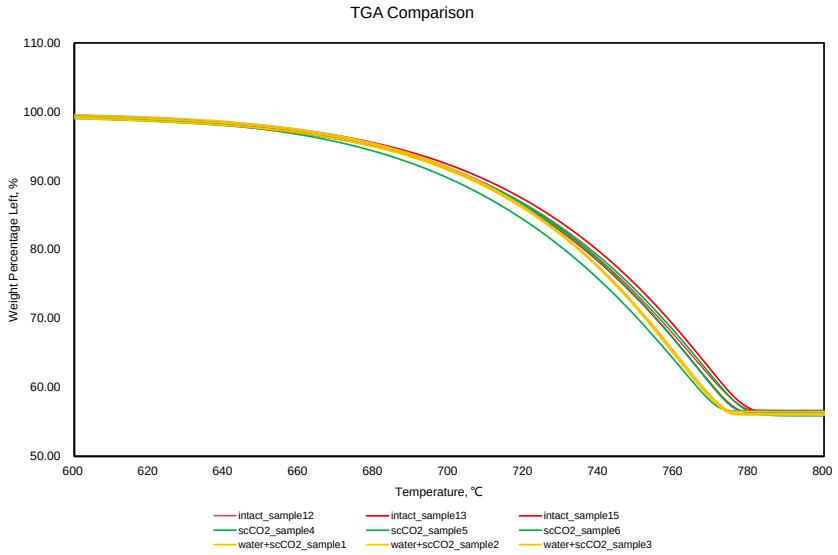

Figure 18. TGA comparison – weight percentage vs temperature.

The next comparable parameter from TGA test is the weight percentage left in y-axis. The weight percentage value after decomposition process from different samples were very close and had just 0.53% and 0.35% decrease in water+$scCO_2$ and $scCO_2$ group compared to intact group respectively. The comparison data is shown in Table 6. The weight percentage measured from different groups were all around 44%, didn't give an obvious change. The process during decomposition can be explained by the equation:

$$CaCO_{3(s)} \xrightarrow{\Delta} CaO_{(s)} + CO_2 \qquad \text{Eq. 26}$$

At a certain temperature, calcium carbonate ($CaCO_3$) will decompose to solid calcium oxide (CaO) and gaseous carbon dioxide (CO_2). The molecular percentage of CO_2 to $CaCO_3$ is 44%, which is the weight loss of this decomposition interaction. And this value is in good agreement with the experimental result obtained in Table 6. It is showing that considering the heterogeneity of the rock, the composition of the core samples didn't change after exposed to $scCO_2$ no matter water existed or not and all the core samples were composed of $CaCO_3$ at a very high percentage before TGA test and CaO after that, with only minority of impurities exist in the samples. This hypothesis would be verified through the following measurements of mineral determination.

Table 6. Comparison data after TGA test.

sample		complete burning temperature, °C	weight before test, mg	weight after test, mg	weight percentage, %
intact	12	781	10	5.66	56.6
	13	783	10	5.62	56.2
	15	781	10	5.63	56.3
	average	**781.6**	**10**	**5.64**	**56.4**
water+scCO2	1	777	10	5.59	55.9
	2	777	10	5.61	56.1
	3	776	10	5.64	56.4
	average	**776.7**	**10**	**5.61**	**56.1**
scCO2	4	774	10	5.65	56.5
	5	779	10	5.63	56.3
	6	782	10	5.58	55.8
	average	**778.3**	**10**	**5.62**	**56.2**

After minus the heat flow of empty alumina crucible in the same method, DSC curves are depicted in Figure 19 and 20 with temperature and time on x-axis respectively. DSC curves indicate a similar trend with TGA. Until the temperature of around 660 °C, the curves started a relatively noticeable change of declination. It signifies that thermal decomposition initiated and the emergence of calcium oxide at this point. And experienced rapid decomposition when it reached to higher temperature. For impure samples, the curve often shows several peaks (Hepzi et al., 2016). One peak in each result could indicate the chalk samples from Stevns Klint have a high purity of calcium carbonate. This is in consistent with TGA result. The peak between 700 and 800 °C in Figure 19 reveals the maximum heat absorption at which point the most decomposition performed here. The point where the intersection of the curve and the x-axis, that's the end of decomposition process. Because of the heterogeneity of chalk and particle size of each sample for DSC test (melting point increases when particle size increases (Hepzi et al., 2016)), the curves even from one group could have differences in value. It is also noticed that in Figure 19 and 20, the DSC results have a clear distinction from different groups (but with an exception of sample 3). This phenomenon is consistent with TGA result that $scCO_2$ could have some influence on thermostability of the chalk. It may be the thermostability difference between calcite and $CaCO_3$ precipitated during interaction. According to some studies, amorphous calcium carbonate (ACC) (chemical composition $CaCO_3 \cdot H_2O$ (L. Goodwin et al., 2010)), can be synthesized in the solution containing dissolved calcium and carbonate ions (L. Goodwin et al., 2010). The difference between water+$scCO_2$ and intact group could be the result of ACC and its crystallization process, during which stage calcite could be formed with vaterite as intermediates (Rodriguez-Blanco et al., 2011). Crystallization of ACC can be either exothermic or endothermic process according to different environment conditions (Koga et al., 1998).

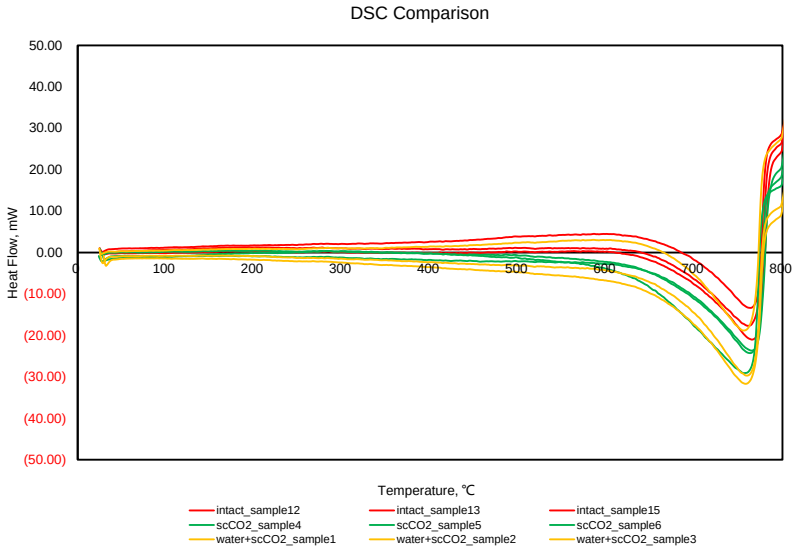

Figure 19. DSC comparison – heat flow with temperature

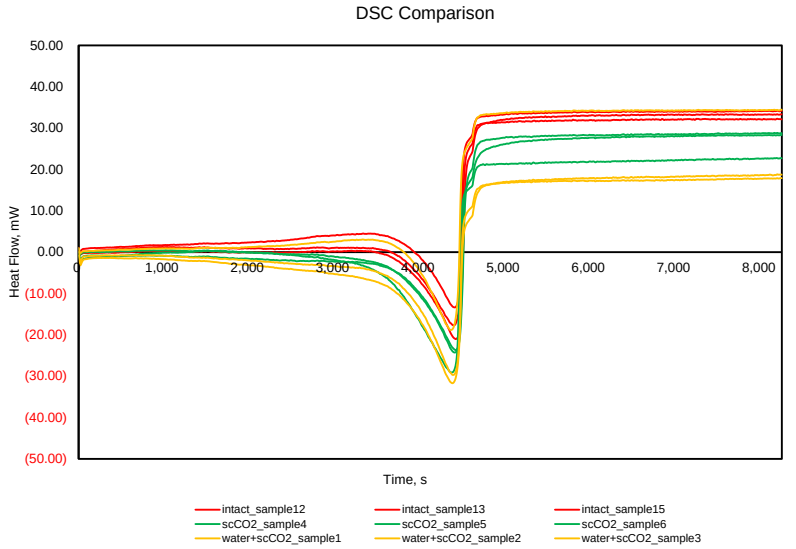

Figure 20. DSC comparison – heat flow with time

4.9. Mineralogy

1. Scanning Electron Microscopy (SEM) & Energy Dispersion Spectrum (EDS).

   The results from SEM at magnification of 3K and 10K are shown in Figure 21 and Figure 22 separately.

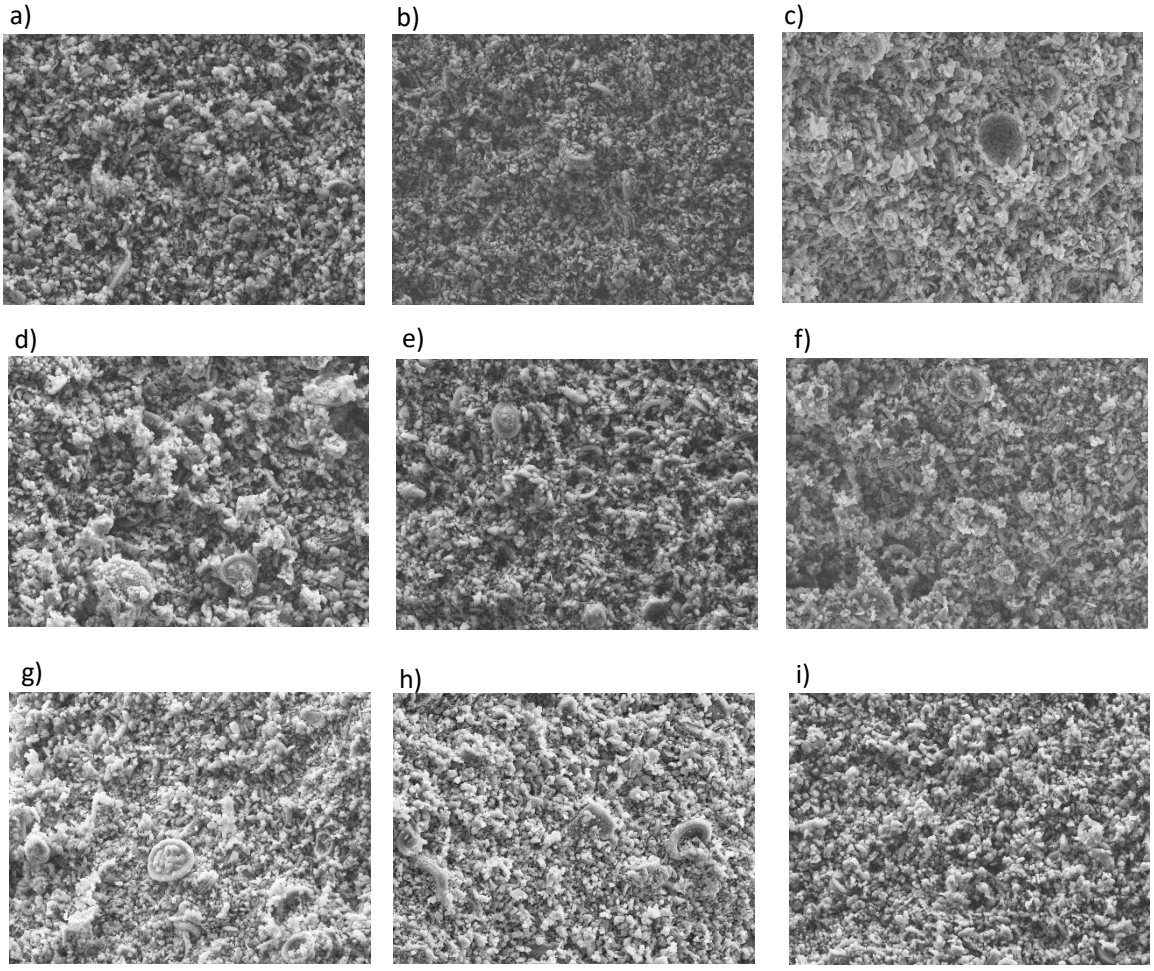

Figure 21. SEM results comparison at magnification of 3K with
a)- sample 1, b)- sample 2, c)- sample 3 in water+scCO_2 group on the first line;
d)- sample 4, e)- sample 5, f)- sample 6 in scCO_2 group on the second line;
and g)- sample 12, h)- sample 13, i)- sample 15 in intact group on the third line.

Shapes of the chalk samples before and after interaction could be observed from SEM images in Figure 21 and Figure 22. There is no big difference between the three groups in terms of pore structure and the type of fossils. There could be several reasons for this phenomenon, the most influential factor should be the interaction time between chalk samples and CO_2. For the interactions including CO_2 dissolution in water, $CaCO_3$ dissolution and precipitation happened slowly, the variation of the chalk samples on the surface was not obvious enough to be observed on grain scale under microscopy within 37-days exposure test. And the other reason could be the fluid used for interaction. Distilled water was used in the CO_2 vessel to simplify the situation in actual environment. That means, no other kinds of ions were added into the interaction and the minerals formed could just the combination of the ions from chalk samples and CO_2 injected. But deepening of surface flatness could still be observed after interaction according to the shadows and contrast of color shades in the images, especially in Figure 21- d), e) and f) of scCO_2 group. This could be explained by dissolution of calcium

carbonate ($CaCO_3$) by $scCO_2$, which made the surface rougher and created more shadows under microscopy. For water+$scCO_2$ group, the reprecipitation of $CaCO_3$ on the surface and in the pore space of rock samples could fill the pore space created by dissolution to some extent, making the surface smoother compared to $scCO_2$ group. It was concluded that the interactions between chalk, $scCO_2$ and distilled water for 37 days didn't noticeably change the nature of the chalk samples.

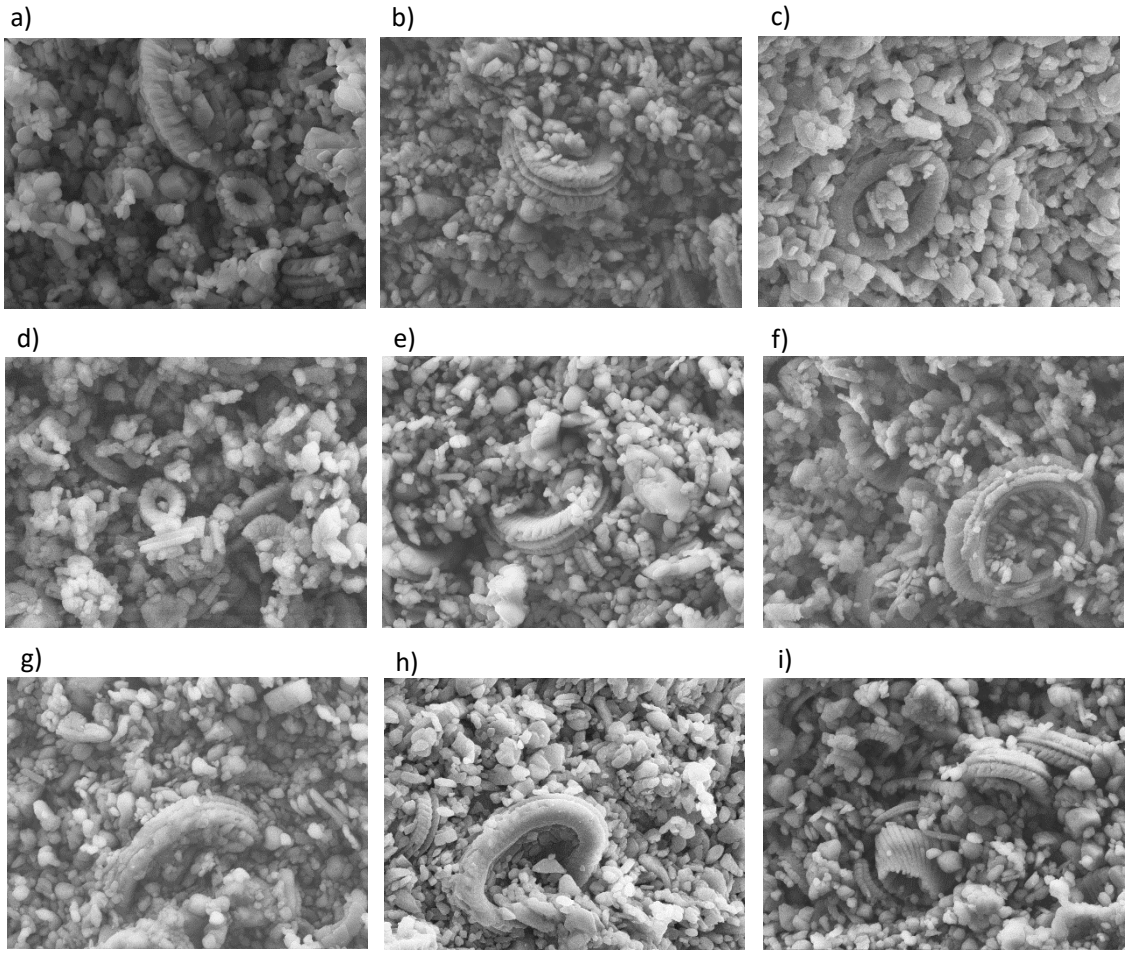

Figure 22. SEM results comparison at magnification of 10K with
a)- sample 1, b)- sample 2, c)- sample 3 in water+$scCO_2$ group on the first line;
d)- sample 4, e)- sample 5, f)- sample 6 in $scCO_2$ group on the second line;
and g)- sample 12, h)- sample 13, i)- sample 15 in intact group on the third line.

The EDS tests were all conducted at magnification of 3K, and the result of weight percentage of each ion is shown in Table 7. All the 9 samples show the result of mostly consisting of Ca, C, O ions and small amount of Mg, Al, Si, and P, which come from impurities. Still no obvious difference between the groups can be distinguished and the fluctuations between each sample could be the heterogeneity of chalk.

Table 7. EDS results of all 9 samples at magnification of 3K.

Weight, % / Element	water+scCO2			scCO2			intact		
	sample 1	sample 2	sample 3	sample 4	sample 5	sample 6	sample 12	sample 13	sample 15
C	3.55	1.61	2.38	3.55	3.34	3.37	3.37	3.8	3.9
O	52.45	36.43	45.94	50.35	51.05	51.57	51.57	52.52	56.25
Mg	0.1	0	0.01	0.03	0.09	0	0	0.15	0.01
Al	0.16	0	0.02	0.03	0.15	0.03	0.03	0.24	0.03
Si	0.44	0	2.29	0.23	0.3	0.13	0.13	0.47	0.17
Ca	43.29	61.96	49.36	45.81	45.06	44.9	44.9	42.62	39.65
P	/	/	/	/	/	/	/	0.2	/

2. X-ray diffraction (XRD)

The results from XRD are shown in Figure 23 and Figure 24. From the two images in Figure 23, the intensity and the position of them in x-axis are almost all the same. It means there was not mineral alteration or new type of mineral created after chalk samples exposed to $scCO_2$. And the tiny differences between each curve could come from contamination created during sample making process, or the differences (compaction degree or surface flatness) between samples (Figure 25-left) prepared for XRD analysis. And even for the same chalk sample, these kinds of tiny differences between curves can occur.

For mineral analysis in Figure 24, all the 9 sample patterns gave the peaks matching the mineral of calcite, which consists of $CaCO_3$. Besides $CaCO_3$, there is another small peak around 26.5 2Theta, which shows existence of SiO_2 according to the database. But it could come from mortar (Figure 25-right, made of agate) for sample preparation. Amorphous materials are often observed as a “broad bump” in the background and couldn’t be easily distinguished in XRD results. Therefore, amorphous calcite carbonate mentioned in the TGA hypothesis couldn’t be proved through XRD. And for most materials, they will produce clear peaks at the minimum amount of a 4-5 % in weight. Therefore, if vaterite was created during interaction with $scCO_2$ but the amount was not high enough, it couldn’t be detected by XRD analysis either.

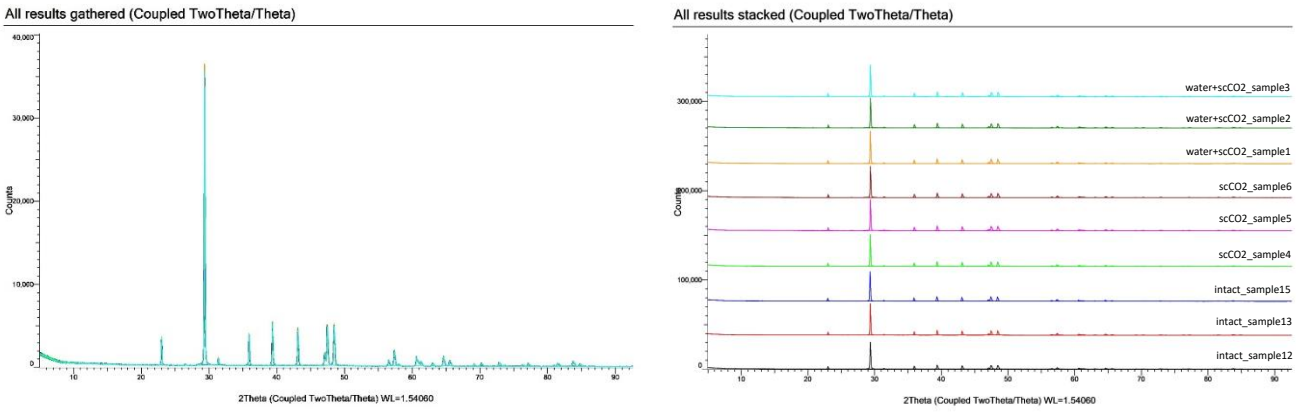

Figure 23. XRD results from 9 samples gathered (left) and stacked (right).

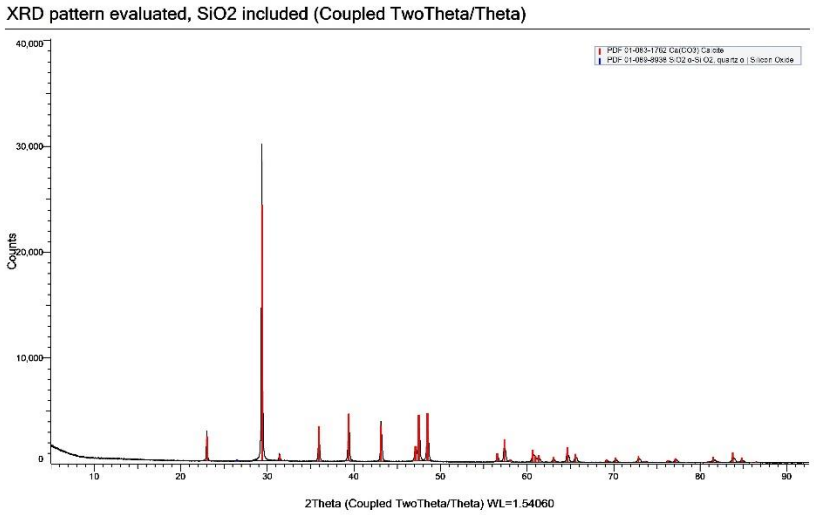

Figure 24. XRD evaluation result.

Figure 25. 9 samples for XRD analysis (left) and mortar for sample preparation (right).

4.10. Uniaxial Compressive Strength (UCS)

For the diameters of the samples were not exactly the same and it could have some effects to the comparison, stress values calculated by using the load values divided by the cross-sectional areas of each specimen were used in the y-axis to compare the mechanical properties. The compared curves are shown in Figure 26. Because the core of sample 5 from $scCO_2$ group was broken in the saturation process, there are 8 curves of the left samples are presented in this stage. The peak load and peak stress of each specimen given by the system are shown in Table 8 and the pictures of samples after UCS tests are shown in Figure 27.

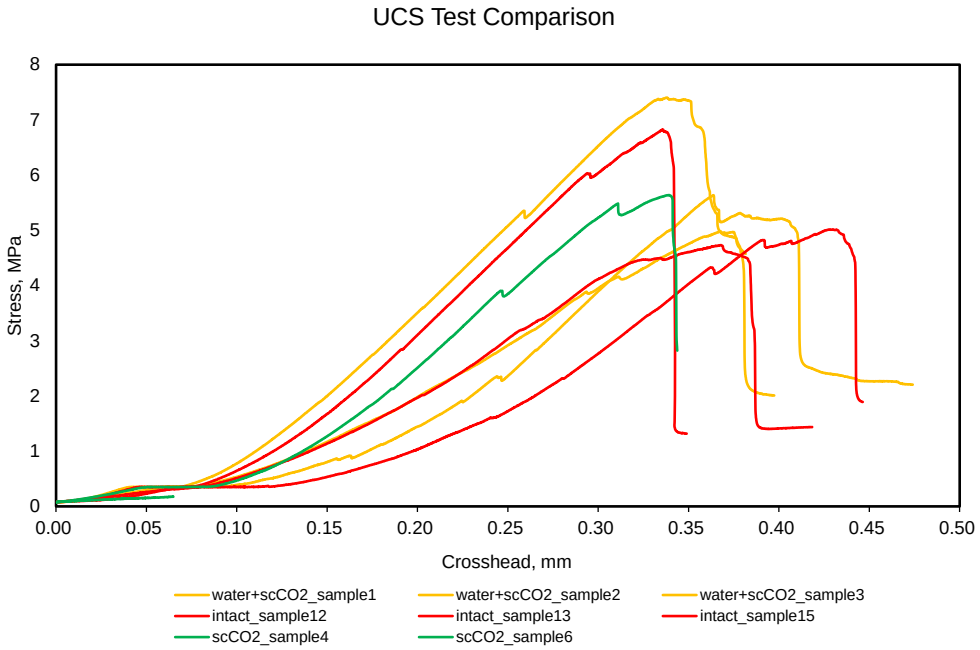

Figure 26. UCS test results.

Table 8. Peak load and peak stress values given by the system.

Sample	Item	peak load, kN	peak stress, Mpa
water+scCO$_2$	1	8.349	7.4
	2	6.366	5.6
	3	5.612	5.0
scCO$_2$	4	6.394	5.6
	5	2.633	2.3
intact	12	7.720	6.8
	13	5.688	5.0
	15	5.350	4.7

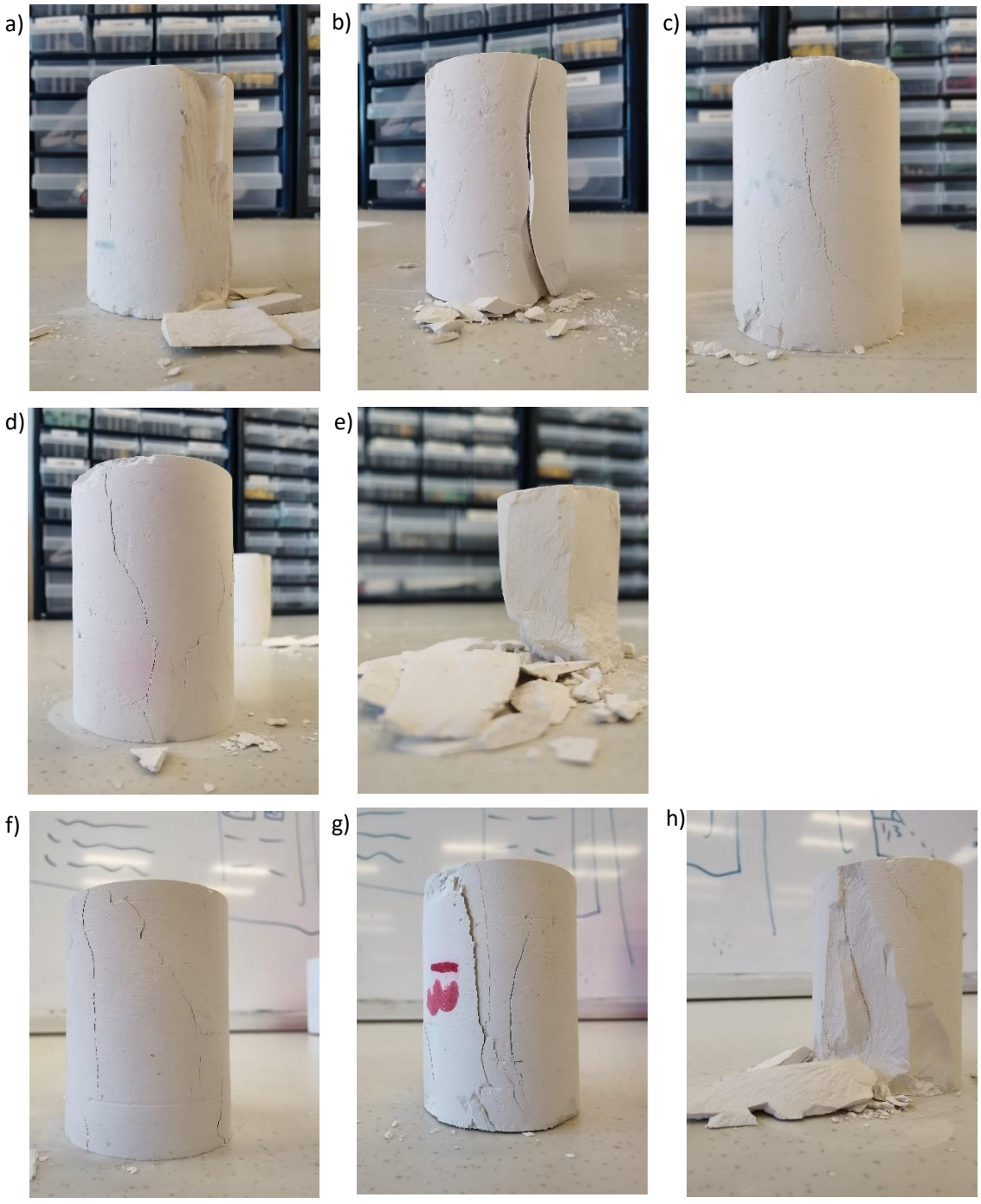

Figure 27. a) sample 1, b) sample 2, c) sample 3 in water+scCO$_2$ group;

d) sample 4, e) sample 6 in scCO$_2$ group;

and f) sample 12, g) sample 13, h) sample 15 in intact group after UCS test.

Comparing the water+scCO$_2$ group curves in yellow and intact group curves in red in Figure 26, the trend of slightly increased peak stress can be observed. It can be explained by the reprecipitation of the calcium carbonate in pore space of the core samples, which may strengthen the specimens to withstand a higher compressive

stress to some extent. As to sample 6 from $scCO_2$ group, the peak load and peak stress were recorded 2.633 kN and 2.3 MPa respectively. But the detailed data was lost due to some technical issues, just stopped at the load of 0.20 kN. So, the $scCO_2$ group in green only has one series of valid data available from sample 4, which has the similar value with sample 2 from water+$scCO_2$ group. Therefore, it couldn't come to any conclusion due to insufficient data. In each curve, there is one or more slight downtrends during their process of ascending could be observed. At that point, there were micro cracks created and it could be observed from the outside of the samples during the UCS test, also the sounds of cracking could be heard at the same time. For example, to sample 15, the left image in Figure 28 shows some obvious cracks. The crack creating time corresponds to the point in Figure 26 (the middle red curve) where crosshead is about 0.34 mm. Comparing the two images in Figure 28, it created longer and maybe deeper cracks at the end of the UCS test and it can be known that the cracks started to be created during the test, not only at the point when the specimen was failed. Wing cracks were generated in Figure 27-left as the test going and when the microstructure of this sample couldn't hinder the propagation of the wing cracks, the specimen failed in axial splitting mode (Chakraborty et al., 2019).

Figure 28. Sample 15 during UCS test (left) and after failure (right).

During the failure process, cracks propagated from the bottom to the top of the chalk samples, shearing off a large piece of the sample. There are mainly 6 failure modes under uniaxial compression: 1) Axial splitting, 2) Shearing along single plane, 3) Double shear, 4) Multiple fracturing, 5) Along foliation, and 6) Y-shaped failure (Chakraborty et al., 2019). The schematic representation of these 6 different failure modes is shown in Figure 29 (Basu et al., 2013). All the eight samples after UCS test in Figure 27 are in failure mode of axial splitting, one of the most common types of failure modes. But for sample 1 in Figure 27-a), there was just a thin spalling of the chalk sample, which may be due to the cross-sectional areas were not even enough. And the failure modes from other 7 samples were more representative to describe mechanical properties of these chalk samples after mechanical grinding. The failure

modes depend on the direction of crack propagation, the distribution of relatively weak zones and the discontinuities in the samples. The rock samples usually fail through fracture planes created in brittle crystalline materials in it (Chakraborty et al., 2019). Comparing the failure modes from these three groups in Figure 27, there is a clear sign that the samples were broken into more fragmented pieces among $scCO_2$ group (second line) and the intact group (third line), compared to the water+$scCO_2$ group (first line). It can also be explained by the reprecipitation process in the solution that more minerals were settled down in the pore space which could surround the relatively weak part like brittle crystalline materials to help the specimens support themselves against axial compressive stress as a whole. The failure modes are in consistent with the UCS results in Figure 26 that the less fragmented cores have withstood relatively higher stress.

But it needs to be noticed that the strength of the rock samples measured in the laboratory usually do not reflect its properties in field scale accurately. Because in the reservoirs, the properties are also influenced by faults, inhomogeneities, joints, weakness planes and other factors (Harbor & Conshohocken, n.d.). Therefore, the results from UCS tests should be dealt with additional evaluation before practical applications.

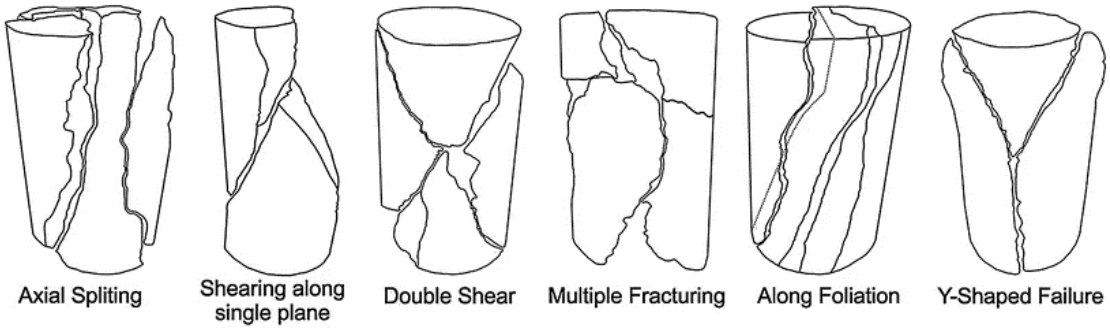

Figure 29. Schematic representation of different failure modes under uniaxial compression

4.11. Conclusion

According to the experiments conducted, porosity, pore size distribution, permeability decreased, and specific surface area and UCS increased after chalk samples exposed to water and $scCO_2$. The results are consistent with each other and the changing trend of these parameters could be explained by the variation of ion concentration in the solution. But not much difference in mineralogy could be distinguished. To the chalks exposed to dry $scCO_2$, not all the parameters could come to a conclusion after interaction.

5. Conclusions and Recommendations

5.1. Conclusions

The CO_2-fluid-chalk experiment was conducted in a sealed stainless-steel vessel for 37 days at pressure of 150 bar and temperature of 50 °C, at which CO_2 was at supercritical state. During the whole experimental process, pH value was the first serious of data obtained and the samples were sent to ICP analysis after that. Other properties like porosity and permeability were conducted after the end of the exposure test. Below are the conclusions reached in this study based on the experimental data.

1) During the exposure test, pH value first gave the information that $scCO_2$ was interacting with distilled water and maybe chalk samples at the same time inside the CO_2 vessel. It decreased from 9.44 (chalk samples soaked in the distilled water before CO_2 injection) to around 6.5 until the end of the exposure test.
2) Stevns Klint chalk has porosity as high as 45% to 60%, and it kept at this level even after interaction with $scCO_2$ and water. Advantages have been seen in terms of storage capacity. However, chalk is ruled out of suitable geological sites by lacking of injectivity due to its low permeability.
3) After interaction with water and $scCO_2$, the parameters including porosity, pore size distribution and permeability decreased, and its specific surface area and UCS increased. The variations could be explained by precipitation of calcium carbonate ($CaCO_3$) inside the pore space, which could be observed from ion concentration of the solution.
4) $scCO_2$ could interact with calcite according to the comparisons of the parameters before and after interaction. But for some properties, there is no consistent trend for the samples in this group. It needs to be mentioned that the $scCO_2$ and water+$scCO_2$ are not isolated from each other in the CO_2 vessel so some water vapor may exist within $scCO_2$ group, which may have some effects.
5) There was no mineral alteration observed after chalk-$scCO_2$ or chalk-water-$scCO_2$ interaction according to XRD and SEM-EDS results. The percentage of weight loss from TGA results was in consistent with it. But slight deepening of flatness could be observed after interactions in SEM images, which could be explained by dissolution of $CaCO_3$ by CO_2.

5.2. Recommendations

This study has some flaws and deficiencies due to time and other restrictions and there were also some problems arose during the experiments. The following is a list of suggestions recommended in the future work.

1) To evaluate the feasibility of chalks as a good storage site, it is recommended to do the exposure test for a longer time. It may get a more accurate prediction according to the property measurement of rock samples from a longer exposure time.
2) Wettability governs the flow behavior in the pore spaces and could have big impact on injectivity and containment during storage stage. Therefore, wettability, as another important property during CCS technology is need to be compared through flooding after CO_2 exposure test as well. More experimental tests for measuring the changes in the capillary pressure and relative permeability over time are also recommended.
3) If the carbonation depth can be measured, the ingression of CO_2 and how the chalks responded to CO_2 exposure could be studied. It will also be helpful to predict CO_2-chalk reaction rate. The pH value of chalk samples itself is not high enough for phenolphthalein to change color to pink, so another acid-base indicator or method should be found.
4) More rock samples are recommended to take into the exposure test, to give sufficient and representative measurement results. And the $scCO_2$ and water+$scCO_2$ group inside the CO_2 vessel are recommended to be isolated from each other, to avoid the water vapor existence during chalk-$scCO_2$ process.

6. Acknowledgements

Foremost, I want to express my sincere appreciation to my supervisor Professor Raoof Gholami, who took me into the CCS world, and gave me professional guide, persistent patience and encouragement all the time.

To Kim Andre Nesse Vorland, Dagfinn Søndenaa Sleveland, Reidar Inge Korsnes, Jorunn Hamre Vrålstad, Ola Ketil Siqveland, Stian Penev Ramsnes, Caroline Ruud and Mona Wetrhus Minde, thank you for your help with my laboratory work. I couldn't fulfill my project without any of your support.

To my friends, in Stavanger and China. Thank you for not letting me feel lonely when I'm happy, sad, or helpless.

Finally, to my parents, thank you for supporting me no matter what kind of decision I make. I love you.

7. References

Advanced Resources International, I. (2000). *BARRIERS TO OVERCOME IN IMPLEMENTATION OF CO2 CAPTURE AND STORAGE (1) - STORAGE IN DISUSED OIL AND GAS FIELDS*. https://ieaghg.org/docs/General_Docs/Reports/PH3_22%20Storage%20in%20oil%20and%20gas%20fields.pdf

Ahmadi, P., & Chapoy, A. (2018). CO2 solubility in formation water under sequestration conditions. *Fluid Phase Equilibria*, *463*, 80–90. https://doi.org/10.1016/J.FLUID.2018.02.002

Ameri, A., Shojai Kaveh, N., S. J. Rudolph, E., Wolf, K., Farajzadeh, R., & Bruining, J. (2013). Investigation on Interfacial Interactions among Crude Oil–Brine–Sandstone Rock–CO2 by Contact Angle Measurements. *Energy & Fuels*, *27*(2), 1015–1025. https://doi.org/10.1021/ef3017915

Amini, S., Mohaghegh, S., Gaskari, R., & Bromhal, G. (2012). *Uncertainty Analysis of a CO2 Sequestration Project Using Surrogate Reservoir Modeling Technique*. https://onepetro.org/SPEWRM/proceedings/12WRM/All-12WRM/SPE-153843-MS/157858

Aminu, M. D., Nabavi, S. A., & Manovic, V. (2018). CO2-brine-rock interactions: The effect of impurities on grain size distribution and reservoir permeability. *International Journal of Greenhouse Gas Control*, *78*, 168–176. https://doi.org/10.1016/J.IJGGC.2018.08.008

Bachu, S., Bonijoly, D., Bradshaw, J., Burruss, R., Holloway, S., Christensen, N. P., & Mathiassen, O. M. (2007). CO2 storage capacity estimation: Methodology and gaps. *International Journal of Greenhouse Gas Control*, *1*(4), 430–443. https://doi.org/10.1016/S1750-5836(07)00086-2

Baines, S. J., & Worden, R. H. (2004). The long-term fate of CO2 in the subsurface: Natural analogues for CO2 storage. *Geological Society Special Publication*, *233*, 59–85. https://doi.org/10.1144/GSL.SP.2004.233.01.06

Bandilla, K. W. (2020). Carbon Capture and Storage. *Future Energy: Improved, Sustainable and Clean Options for Our Planet*, 669–692. https://doi.org/10.1016/B978-0-08-102886-5.00031-1

Banerjee, D. (n.d.). *Experimental Techniques in Thermal Analysis Thermogravimetry (TG) & Differential Scanning Calorimetry (DSC)*. Retrieved May 11, 2022, from https://www.iitk.ac.in/che/pdf/resources/TGA-DSC-reading-material.pdf?msclkid=6a09fda1d12911ec9acc44692600f0f5

Basu, A., Mishra, D. A., & Roychowdhury, K. (2013). Rock failure modes under uniaxial compression, Brazilian, and point load tests. *Bulletin of Engineering Geology and the Environment*, *72*(3–4), 457–475. https://doi.org/10.1007/S10064-013-0505-4/FIGURES/18

BET Specific Surface Area - Particle Technology Labs. (n.d.). Retrieved May 25, 2022, from https://www.particletechlabs.com/analytical-testing/gas-adsorption-and-porosimetry/bet-specific-surface-area

BET theory - Wikipedia. (n.d.). Retrieved May 25, 2022, from https://en.wikipedia.org/wiki/BET_theory

BP p.l.c. (2021). *Statistical Review of World Energy 2021 - 70th edition*.

https://www.bp.com/content/dam/bp/business-sites/en/global/corporate/pdfs/energy-economics/statistical-review/bp-stats-review-2021-full-report.pdf

Carbon Capture & Storage - CCS research from SINTEF. (n.d.). Retrieved May 12, 2022, from https://www.sintef.no/en/sintef-research-areas/ccs/

Chakraborty, S., Bisai, R., Palaniappan, S. K., & Pal, S. K. (2019). *Failure Modes of Rocks under Uniaxial Compression Tests: An Experimental Approach*. https://doi.org/10.5281/ZENODO.3461773

Costa, A. (2006). Permeability-porosity relationship: A reexamination of the Kozeny-Carman equation based on a fractal pore-space geometry assumption. *Geophysical Research Letters*, *33*(2). https://doi.org/10.1029/2005GL025134

Crockford, P., & Telmer, K. (2011). Dissolution Kinetics of Keg River dolomites and implications for spectra energy's Fort Nelson CCS project. *Energy Procedia*, *4*, 4472–4479. https://doi.org/10.1016/J.EGYPRO.2011.02.402

Definition > Saline aquifer. (n.d.). Retrieved May 12, 2022, from http://www.futura-sciences.us/dico/d/geology-saline-aquifer-50005366/

di Gianfrancesco, A. (2017). Worldwide overview and trend for clean and efficient use of coal. *Materials for Ultra-Supercritical and Advanced Ultra-Supercritical Power Plants*, 643–687. https://doi.org/10.1016/B978-0-08-100552-1.00019-1

Doctor, R., Palmer, A., Coleman, D., Davison, J., Hendriks, C., Kaarstad, O., Ozaki, M., & Austell, M. (2018). *IPCC Special Report on Carbon dioxide Capture and Storage*. https://www.ipcc.ch/site/assets/uploads/2018/03/srccs_chapter4-1.pdf

ECMWF. (2017). *Main sources of carbon dioxide emissions*. https://www.che-project.eu/news/main-sources-carbon-dioxide-emissions

EPA. (n.d.). *Overview of Greenhouse Gases*. Retrieved February 3, 2022, from https://www.epa.gov/ghgemissions/overview-greenhouse-gases

Espinoza, D. N., Kim, S. H., & Santamarina, J. C. (2011). CO 2 Geological Storage − Geotechnical Implications. *KSCE Journal of Civil Engineering*, *15*(4), 707–719. https://doi.org/10.1007/s12205-011-0011-9

Faleide, J. I., Bjørlykke, K., & Gabrielsen, R. H. (2015). Geology of the norwegian continental shelf. *Petroleum Geoscience: From Sedimentary Environments to Rock Physics, Second Edition*, 603–635. https://doi.org/10.1007/978-3-642-34132-8_25/FIGURES/20

Finney, K. N., Akram, M., Diego, M. E., Yang, X., & Pourkashanian, M. (2019). Carbon capture technologies. *Bioenergy with Carbon Capture and Storage: Using Natural Resources for Sustainable Development*, 15–45. https://doi.org/10.1016/B978-0-12-816229-3.00002-8

Foroutan, M., Ghazanfari, E., Amirlatifi, A., & Moradian, O. (2021). Evolution of fracture permeability and aperture during CO2 storage in varyingly cemented sedimentary rocks. *Geomechanics for Energy and the Environment*, 100289. https://doi.org/10.1016/J.GETE.2021.100289

Frykman, P., Jacobsen, F., & Surlyk, F. (2004). *The chalk at Stevns Klint - A reservoir chalk analogue?* https://data.geus.dk/pure-pdf/25636_GEUS_R_2004_56_opt.pdf

García-Rios, M., Luquot, L., Soler, J. M., & Cama, J. (2013). Laboratory-Scale Interaction between CO2-Rich Brine and Reservoir Rocks (Limestone and Sandstone). *Procedia Earth and Planetary Science*, *7*, 109–112. https://doi.org/10.1016/J.PROEPS.2013.03.013

Gaus, I. (2010). Role and impact of CO2–rock interactions during CO2 storage in sedimentary rocks. *International Journal of Greenhouse Gas Control*, *4*(1), 73–89. https://doi.org/10.1016/J.IJGGC.2009.09.015

Global CCS Institute. (n.d.-a). *Capturing carbon dioxide (CO2)*. Retrieved March 31, 2022, from https://www.globalccsinstitute.com/about/what-is-ccs/capture/

Global CCS Institute. (n.d.-b). *Understanding CCS-Storage*. Retrieved February 7, 2022, from https://www.globalccsinstitute.com/about/what-is-ccs/transport/

Goldthorpe, S. (2017). Potential for Very Deep Ocean Storage of CO2 Without Ocean Acidification: A Discussion Paper. *Energy Procedia*, *114*, 5417–5429. https://doi.org/10.1016/J.EGYPRO.2017.03.1686

Green Facts. (2005). *CO2 Capture and Storage*. Green Facts. https://www.greenfacts.org/en/co2-capture-storage/l-3/4-transport-carbon-dioxide.htm

Harbor, B., & Conshohocken, W. (n.d.). *Standard Test Method for Unconfined Compressive Strength of Intact Rock Core Specimens*.

Hedges, S. W., Soong, Y., Jones, J. R. M. C., Harrison, D. K., Irdi, G. A., Frommell, E. A., Dilmore, R. M., & White, C. M. (2007). Exploratory study of some potential environmental impacts of CO2 sequestration in unmineable coal seams. *International Journal of Environment and Pollution*, *29*(4), 457–473. https://doi.org/10.1504/IJEP.2007.014232

Hepple, R. P., & Benson, S. M. (2005). Geologic storage of carbon dioxide as a climate change mitigation strategy: performance requirements and the implications of surface seepage. *Environmental Geology*, *47*(4), 576–585. https://doi.org/10.1007/s00254-004-1181-2

Hepzi, R., Devamani, P., Deepa, N., & Gayathri, J. (2016). Morphology and Thermal Studies of Calcium Carbonate Nanoparticles. *IJISET-International Journal of Innovative Science, Engineering & Technology*, *3*(1). https://ijiset.com/vol3/v3s1/IJISET_V3_I1_12.pdf

Höhne, G. W. H., Breuer, K. H., & Eysel, W. (1983). Differential scanning calorimetry: Comparison of power compensated and heat flux instruments. *Thermochimica Acta*, *69*(1–2), 145–151. https://doi.org/10.1016/0040-6031(83)85073-4

Iglauer, S. (2017). CO2–Water–Rock Wettability: Variability, Influencing Factors, and Implications for CO2 Geostorage. *Accounts of Chemical Research*, *50*(5), 1134–1142. https://doi.org/10.1021/acs.accounts.6b00602

Jacques, P. M., Professeur, L., Rapporteurs, N. I., & Gilles Berger, : M. (n.d.). *Durabilité des matériaux de puits pétroliers dans le cadre d'une séquestration géologique de dioxyde de carbone et d'hydrogène sulfuré Laboratoire de Géologie et Gestion des Ressources Minérales et Energétiques Faculté des Sciences & Techniques-54500 Vandoeuvre-lès-Nancy*. Retrieved June 5, 2022, from https://www.osti.gov/etdeweb/servlets/purl/20972267

Kahan, A. (2019). *EIA projects nearly 50% increase in world energy usage by 2050, led by growth in Asia*.

Karunadasa, K. S. P., Manoratne, C. H., Pitawala, H. M. T. G. A., & Rajapakse, R. M. G. (2019).

Thermal decomposition of calcium carbonate (calcite polymorph) as examined by in-situ high-temperature X-ray powder diffraction. *Journal of Physics and Chemistry of Solids*, *134*, 21–28. https://doi.org/10.1016/J.JPCS.2019.05.023

Koga, N., Nakagoe, Y., & Tanaka, H. (1998). Crystallization of amorphous calcium carbonate. *Thermochimica Acta*, *318*(1–2), 239–244. https://doi.org/10.1016/S0040-6031(98)00348-7

L. Goodwin, A., Marc Michel, F., L. Phillips, B., A. Keen, D., T. Dove, M., & J. Reeder, R. (2010). Nanoporous Structure and Medium-Range Order in Synthetic Amorphous Calcium Carbonate. *Chemistry of Materials*, *22*(10), 3197–3205. https://doi.org/10.1021/cm100294d

Li, S., Zhang, S., Zou, Y., Ma, X., Ding, Y., Li, N., Zhang, X., & Kasperczyk, D. (2020). Pore structure alteration induced by CO2–brine–rock interaction during CO2 energetic fracturing in tight oil reservoirs. *Journal of Petroleum Science and Engineering*, *191*, 107147. https://doi.org/10.1016/J.PETROL.2020.107147

Lin, R., Yu, Z., Zhao, J., Dai, C., Sun, Y., Ren, L., & Xie, M. (2022). Experimental evaluation of tight sandstones reservoir flow characteristics under CO2–Brine–Rock multiphase interactions: A case study in the Chang 6 layer, Ordos Basin, China. *Fuel*, *309*, 122167. https://doi.org/10.1016/J.FUEL.2021.122167

Lindeberg, E., & Wessel-Berg, D. (1997). Vertical convection in an aquifer column under a gas cap of CO2. *Energy Conversion and Management*, *38*(SUPPL. 1), S229–S234. https://doi.org/10.1016/S0196-8904(96)00274-9

Metz, B., Davidson, O., Coninck, H. de, Loos, M., & Meyer, L. (n.d.). *Carbon Dioxide Capture and Storage — IPCC*. Retrieved May 12, 2022, from https://www.ipcc.ch/report/carbon-dioxide-capture-and-storage/

NOAA National Centers for Environmental Information. (2022). *State of the Climate: Global Climate Report for 2021*. https://www.ncdc.noaa.gov/sotc/global/202113/supplemental/page-1

Nolan, T. B. (n.d.). *Porosity and Bulk Density of Sedimentary Rocks*. Retrieved May 7, 2022, from https://pubs.usgs.gov/bul/1144e/report.pdf#:~:text=Average%20%20values%20for%20%20the%20porosity%20of,for%20the%20porosity%20of%20shale%20may%20be%20low.

Norwegian Petroleum. (2020, January 27). *CARBON CAPTURE AND STORAGE*. https://www.norskpetroleum.no/en/environment-and-technology/carbon-capture-and-storage/

Nyquist, S. (2016, November 4). *Energy 2050: Insights from the ground up*. https://www.mckinsey.com/industries/oil-and-gas/our-insights/energy-2050-insights-from-the-ground-up#:~:text=By%202050,%20the%20research%20estimates%20that%20coal%20will,primary%20energy%20demand,%20down%20from%2082%20percent%20now.

Oxford Instruments. (2022). *Using NMR to Determine Pore Size Distribution*. https://nmr.oxinst.com/application-detail/pore-size-distribution

Rabbani, A., Jamshidi, S., & Salehi, S. (2014). Determination of Specific Surface of Rock Grains by 2D Imaging. *Journal of Geological Research*, *2014*, 1–7. https://doi.org/10.1155/2014/945387

Rackley, S. A. (2017). Geochemical and biogeochemical features, events, and processes. *Carbon Capture and Storage*, 365–386. https://doi.org/10.1016/B978-0-12-812041-5.00014-3

Regnault, O., Lagneau, V., Catalette, H., & Schneider, H. (2005). Étude expérimentale de la réactivité du CO2 supercritique vis-à-vis de phases minérales pures. Implications pour la séquestration géologique de CO2. *Comptes Rendus Geoscience*, *337*(15), 1331–1339. https://doi.org/10.1016/J.CRTE.2005.07.012

Ringrose, P. (n.d.). *SPRINGER BRIEFS IN EARTH SCIENCES How to Store CO 2 Underground: Insights from early-mover CCS Projects*. Retrieved May 19, 2022, from http://www.springer.com/series/8897

Rodriguez-Blanco, J. D., Shaw, S., & Benning, L. G. (2011). The kinetics and mechanisms of amorphous calcium carbonate (ACC) crystallization to calcite , via vaterite. *Nanoscale*, *3*(1), 265–271. https://doi.org/10.1039/C0NR00589D

Schaef, H. T., McGrail, B. P., & Owen, A. T. (2011). Basalt reactivity variability with reservoir depth in supercritical CO 2 and aqueous phases. *Energy Procedia*, *4*, 4977–4984. https://doi.org/10.1016/J.EGYPRO.2011.02.468

SINTEF. (n.d.). *CCS*. SINTEF. Retrieved February 23, 2022, from https://www.sintef.no/en/shared-research-areas/ccs/

Snæbjörnsdóttir, S., Sigfússon, B., Marieni, C., Goldberg, D., Gislason, S. R., & Oelkers, E. H. (2020). Carbon dioxide storage through mineral carbonation. *Nature Reviews Earth & Environment 2020 1:2*, *1*(2), 90–102. https://doi.org/10.1038/s43017-019-0011-8

Snæbjörnsdóttir, S., Wiese, F., Fridriksson, T., Ármansson, H., Einarsson, G. M., & Gislason, S. R. (2014). CO2 storage potential of basaltic rocks in Iceland and the oceanic ridges. *Energy Procedia*, *63*, 4585–4600. https://doi.org/10.1016/J.EGYPRO.2014.11.491

Specific surface area of porous rocks: an integrated approach by combination of BET and Micro-CT imaging - NASA/ADS. (n.d.). Retrieved June 1, 2022, from https://ui.adsabs.harvard.edu/abs/2012EGUGA..14.7173M/abstract

Sun, L. (n.d.). *Study on the Dissolution on Calcium Carbonate*. Retrieved June 10, 2022, from https://www.docin.com/p-1625634516.html

Sun, Y., Wei, L., Dai, C., Yu, Z., & Xin, Y. (2021). The carbonic acid-rock reaction in feldspar/dolomite-rich tightsand and its impact on CO2-water relative permeability during geological carbon storage. *Chemical Geology*, *584*, 120527. https://doi.org/10.1016/J.CHEMGEO.2021.120527

Tartarello, M. C., Plaisant, A., Bigi, S., Beaubien, S. E., Graziani, S., Lombardi, S., Ruggiero, L., de Angelis, D., Sacco, P., & Maggio, E. (2017). Preliminary results of geological characterization and geochemical monitoring of Sulcis Basin (Sardinia), as a potential CCS site. *Energy Procedia*, *125*, 549–555. https://doi.org/10.1016/J.EGYPRO.2017.08.190

Tawiah, P., Duer, J., Bryant, S., Larter, S., OBrien, S., & Dong, M. (2020). Co2 Injectivity Behaviour - Field Observations from the Quest CCS Operations. *SSRN Electronic Journal*. https://doi.org/10.2139/SSRN.3365776

The Climate Reality Project. (2021). *THE CLIMATE CRISIS IN 2021: 5 KEY FACTS TO KNOW*. https://www.climaterealityproject.org/blog/climate-crisis-2021-5-key-facts-know

Tiseo, I. (2020, October 7). *Forecast of carbon dioxide emissions worldwide from 2018 to 2050*. Statista. https://www.statista.com/statistics/263980/forecast-of-global-carbon-dioxide-emissions/

Unconfined Compression Test | Geoengineer.org. (n.d.). Retrieved May 25, 2022, from https://www.geoengineer.org/education/laboratory-testing/unconfined-compression-test

U.S. Energy Information Administration. (2021, October 6). *INTERNATIONAL ENERGY OUTLOOK 2021*. https://www.eia.gov/outlooks/ieo/introduction/sub-topic-01.php

Wang, F., Ping, S., Yuan, Y., Sun, Z., Tian, H., & Yang, Z. (2021). Effects of the mechanical response of low-permeability sandstone reservoirs on CO2 geological storage based on laboratory experiments and numerical simulations. *Science of The Total Environment*, *796*, 149066. https://doi.org/10.1016/J.SCITOTENV.2021.149066

Wang, H., Alvarado, V., Bagdonas, D. A., McLaughlin, J. F., Kaszuba, J. P., Grana, D., Campbell, E., & Ng, K. (2021). Effect of CO2-brine-rock reactions on pore architecture and permeability in dolostone: Implications for CO2 storage and EOR. *International Journal of Greenhouse Gas Control*, *107*, 103283. https://doi.org/10.1016/J.IJGGC.2021.103283

Wikipedia. (2021, September 22). *Thermostability*. https://en.wikipedia.org/wiki/Thermostability

Wikipedia. (2022a, January 31). *Paris Agreement*. https://en.wikipedia.org/wiki/Paris_Agreement

Wikipedia. (2022b, February 23). *Permeabiltiy*. https://en.wikipedia.org/wiki/Permeability_(Earth_sciences)

Withjack, E. M., Devier, C., & Michael, G. (2003). The Role of X-Ray Computed Tomography in Core Analysis. *SPE Western Regional/AAPG Pacific Section Joint Meeting*, 41–52. https://doi.org/10.2118/83467-MS

World Mapper. (n.d.). *Population Year 2050*. World Mapper. Retrieved February 7, 2022, from https://worldmapper.org/maps/population-year-2050/

X-Ray Diffraction for Determining Atomic and Molecular Structure | Materials Engineering | JoVE. (n.d.). Retrieved May 9, 2022, from https://www.jove.com/v/10446/x-ray-diffraction

Young Upstarts. (2021, April 6). *Everything You Need To Know About the Effects Of Carbon Emissions*. Young Upstarts. https://www.youngupstarts.com/2021/04/06/everything-you-need-to-know-about-the-effects-of-carbon-emissions/

Zero Emission Resource Organisation. (2016). *Carbon Capture and Storage*. https://zero.no/wp-content/uploads/2016/06/carbon-capture-and-storage.pdf

Zhang, D., & Song, J. (2014). Mechanisms for Geological Carbon Sequestration. *Procedia IUTAM*, *10*, 319–327. https://doi.org/10.1016/j.piutam.2014.01.027

Zhang, Y., Zhang, Z., Arif, M., Lebedev, M., Busch, A., Sarmadivaleh, M., & Iglauer, S. (2020). Carbonate rock mechanical response to CO2 flooding evaluated by a combined X-ray computed tomography – DEM method. *Journal of Natural Gas Science and Engineering*, *84*, 103675. https://doi.org/10.1016/J.JNGSE.2020.103675

Zhao, D. F., Liao, X. W., & Yin, D. D. (2015). An experimental study for the effect of CO2-brine-rock interaction on reservoir physical properties. *Journal of the Energy Institute*, *88*(1), 27–35.

https://doi.org/10.1016/J.JOEI.2014.05.001